Cell Reports

Article

# RLI2 regulates *Arabidopsis* female gametophyte and embryo development by facilitating the assembly of the translational machinery

## Graphical abstract

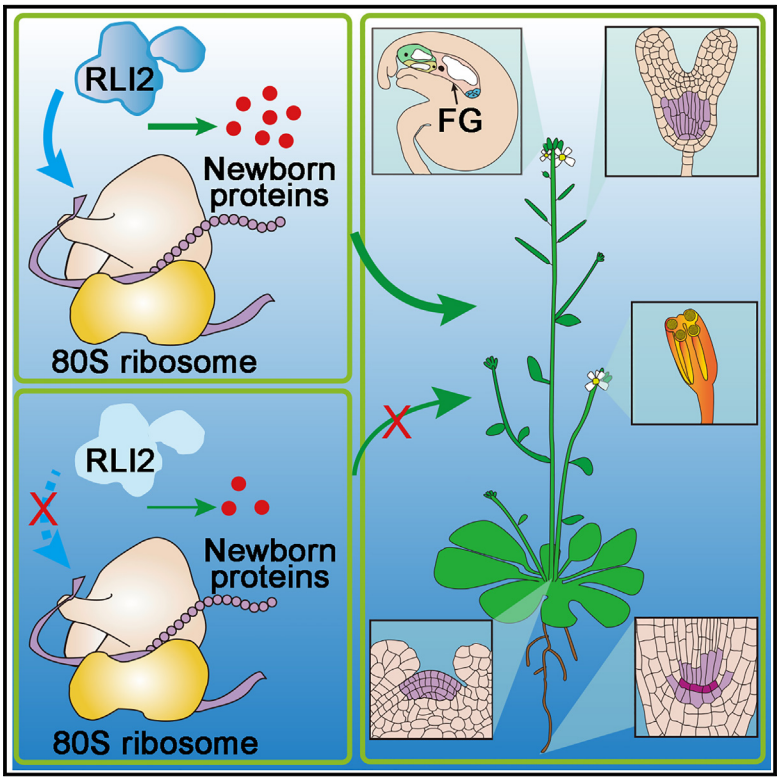


## Highlights

- RLI2 regulates the development of female gametophyte and embryo in *Arabidopsis*
- RLI2 interacts with translation-related factors to regulate translational efficiency
- RLI2 indirectly regulates the expression of genes involved in auxin signaling

## Authors

Shi-Xia Yu, Li-Qin Hu, Lu-Han Yang, ..., Yan-Jie Zhang, Zhi-Ping Xie, Wen-Hui Lin

## Correspondence

whlin@sjtu.edu.cn

## In brief

Yu et al. report that RNase L inhibitor 2/ATP-BINDING CASSETTE E2 (RLI2/ABCE2), which belongs to the evolutionarily conserved RLI/ABCE protein subfamily, regulates female gametophyte and embryo development. RLI2 interacts with several translation-related factors, facilitates translational machinery assembly, and modulates translational efficiency of proteins involved in translation regulation and embryo development.

Yu et al., 2023, Cell Reports *42*, 112741
July 25, 2023 
https://doi.org/10.1016/j.celrep.2023.112741

CellPress

Cell Reports

CellPress
OPEN ACCESS

Article

# RLI2 regulates *Arabidopsis* female gametophyte and embryo development by facilitating the assembly of the translational machinery

Shi-Xia Yu,[1,2,3,5] Li-Qin Hu,[1,2,3,5] Lu-Han Yang,[1] Tao Zhang,[1] Ruo-Bing Dai,[4] Yan-Jie Zhang,[1] Zhi-Ping Xie,[1] and Wen-Hui Lin[1,2,6,*]

[1]The Joint International Research Laboratory of Metabolic and Developmental Sciences, School of Life Sciences and Biotechnology, Shanghai Jiao Tong University, Shanghai 200240, China
[2]Shanghai Collaborative Innovation Center of Agri-Seeds/Joint Center for Single Cell Biology, Shanghai Jiao Tong University, Shanghai 200240, China
[3]School of Agriculture and Biology, Shanghai Jiao Tong University, Shanghai 200240, China
[4]Zhiyuan College, Shanghai Jiao Tong University, Shanghai 200240, China
[5]These authors contributed equally
[6]Lead contact
*Correspondence: whlin@sjtu.edu.cn
https://doi.org/10.1016/j.celrep.2023.112741

## SUMMARY

Eukaryotic protein translation is a complex process that requires the participation of different proteins. Defects in the translational machinery often result in embryonic lethality or severe growth defects. Here, we report that RNase L inhibitor 2/ATP-BINDING CASSETTE E2 (RLI2/ABCE2) regulates translation in *Arabidopsis thaliana*. Null mutation of *rli2* is gametophytic and embryonic lethal, whereas knockdown of *RLI2* causes pleiotropic developmental defects. RLI2 interacts with several translation-related factors. Knockdown of *RLI2* affects the translational efficiency of a subset of proteins involved in translation regulation and embryo development, indicating that RLI2 has critical roles in these processes. In particular, RLI2 knockdown mutant exhibits decreased expression of genes involved in auxin signaling and female gametophyte and embryo development. Therefore, our results reveal that RLI2 facilitates assembly of the translational machinery and indirectly modulates auxin signaling to regulate plant growth and development.

## INTRODUCTION

The process of eukaryotic translation can be divided into four steps: initiation, elongation, termination, and ribosome recycling. These steps require different accessory factors. Compared to transcriptional regulation, translational control of existing mRNAs allows for more rapid changes in the cellular concentrations of the encoded proteins.[1] Most translational regulation occurs during the initiation step.[1] In eukaryotes, the canonical model of translation initiation starts with the assembly of a ternary complex (eIF2-Met-tRNAi-GTP) consisting of methionyl initiator transfer RNA (Met-tRNAi), eukaryotic initiation factor 2 (eIF2), and GTP (guanosine-5′-triphosphate).[2,3] eIF1, eIF1A, eIF3, and eIF5 promote the association of the ternary complex with the 40S ribosomal subunit to form the 43S pre-initiation complex.[2,3] The 43S complex scans the 5′ untranslated regions (UTRs) of genes in the 5′→3′ direction.[2,3] The eIF4F complex then recruits the 5′ UTR to assemble the 48S scanning ribosome.[4,5] Following recognition of the initiation codon, eIF5 and eIF5B promote the hydrolysis of eIF2-bound GTP, the displacement of eIFs, and the joining of a 60S subunit.[2] Some initiation factors also control termination and can even promote ribosome recycling.[6] The ATP-binding cassette (ABC) protein ABCE1 participates in the assembly of the translation initiation complex,[7–9] translation termination, and ribosomal recycling in yeast and animals.[10–13]

ABC proteins, which are present in all living organisms, constitute one of the largest known protein families.[14] ABC proteins are essential for plant development, functioning in gametogenesis, seed development, seed germination, organ formation, and secondary growth.[15–17] Most ABC proteins function as membrane transporters that can transport multiple materials against concentration gradients.[16] Among these, ABCE subfamily members are soluble proteins that lack transmembrane domains. The ABCE subfamily consists of one or two members in different species.[14] *Arabidopsis thaliana* contains two ABCE paralogs (*AtABCE1* and *AtABCE2*).[18] ABCE protein was initially identified as RNase L inhibitor (RLI) protein, a component of the interferon-induced mammalian 2′-5′ oligoadenylate (2-5A) anti-viral pathway.[19]

The role of RLI/ABCE in development has been extensively studied in various species. In yeast, depletion of RLI1 leads to cessation of growth, a lower polysome content, and decreased average polysome size.[9] The fruit fly (*Drosophila melanogaster*)

gene *pixie*, an ortholog of *RLI*, encodes a protein that binds to 40S ribosomes and is required for translation initiation.[7,20] Null *pixie* alleles are recessive-lethal, whereas hypomorphic alleles exhibit severely delayed growth.[7,20] RNAi against *ABCE* resulted in embryonic lethality and slow growth in nematode (*Caenorhabditis elegans*).[21] Inhibition of *Xenopus laevis ABCE1* led to arrested growth at the gastrula stage of development due to a block in translation.[8]

Relatively few studies of RLI/ABCE have been performed in plants. Silencing the *RLI* homolog by virus-induced gene silencing in *Nicotiana benthamiana* resulted in reduced growth and distorted leaves with white spots.[22] In *Cardamine hirsuta*, *SIMPLE LEAF 3* (*SLI3*) encodes RLI2, which is required for leaf growth and leaflet formation.[23] AtRLI2 acts as an endogenous suppressor of RNA silencing, as it drastically reduced the levels of small interfering RNAs when infiltrated into *N. benthamiana*.[18,24] However, no *RLI* mutants have been described in *Arabidopsis*, and the roles of *RLI* in gametophyte development, embryo organogenesis, and meristem formation remain unclear.

Plant life cycles are characterized by the alternation of generations, including haploid generation (female gametophyte, also called embryo sac, and male gametophyte, also named pollen grain) and diploid generation (sporophyte).[25,26] After the gametophyte matures the pollen adheres to the stigma, and the pollen tube grows to transport the sperm cells into the embryo sac.[25] Sperm cell and egg cell fuse to form a zygote, followed by embryo development, which gives rise to the sporophyte.[25,27] During these processes, cells require fine-tuned regulation of gene expression in order to divide, differentiate, and undergo morphogenesis. Translational control is an important part of this regulation.

Recently, several studies demonstrated that genes involved in ribosome biogenesis and the translation process play critical roles in gametophytic and embryo development in *Arabidopsis*. These genes consist of co-factor of ribosome biogenesis *Nin1* (*one*) *binding protein 1* (*NOB1*),[28] *Arabidopsis nucleolar Pumilio 24* (*APUM24*),[29] *SLOW WALKER 1* (*SWA1*),[30] *SWA2*,[31] two DEAD-box RNA helicases *AtRH36* and *SWA3*,[32,33] *ERA-related GTPase 2* (*ERG2*),[34] *MIDASIN1* (*AtMDN1*)-*NOTCHLESS* (*AtNLE*) module,[35] and *KETCH1-ribosomal protein L27a* (*RPL27a*) module.[36] Mutants of these genes display similar reproductive developmental defects. Although these results demonstrated the importance of ribosome biogenesis and the translation process, how these processes are regulated is poorly understood.

In this study, we demonstrate that *Arabidopsis* RLI2 is a conserved factor in the translational machinery that is critical for growth and development. Loss of function of *RLI2* caused the arrest of gametophyte and embryo development, resulting in reduced fertility. A knockdown mutant of *RLI2* generated by RNAi strategy exhibited pleiotropic developmental defects and imbalanced polyribosome profiles, which are characteristic of mutants with translational defects. RLI2 interacts with a few eIFs, and similar phenotypes observed in *RLI2* knockdown mutant have been reported in some *Arabidopsis* eIF mutants. Proteomics analysis illustrated that the translation-related proteins exhibited altered translational efficiency in *RLI2* knockdown mutant, providing insights into the importance of RLI2 for the translational machinery. Using RNA sequencing (RNA-seq) we identified subsets of auxin-related genes, which play prominent roles in plant development, that were downregulated in *RLI2* knockdown mutant. Our findings reveal an important link between RLI2 and the translational machinery, which is essential for plant development in *Arabidopsis*.

## RESULTS

### Loss of function of *RLI2* leads to reduced fertility

To identify novel regulators of fertility, we characterized *RLI2* (AT4G19210), which encodes an *Arabidopsis* ABCE protein whose function in plant development has not been studied. We identified the transfer DNA insertion mutant CS332419, which was renamed as *rli2-1* after genotyping (Figures 1A and 1B). Since the *rli2-1* homozygous mutant (*rli2-1*/−) could not be isolated from self-fertilized *rli2-1* heterozygous plants (*rli2-1*/+) and *rli2-1*/+ displayed no developmental defects at the vegetative stage but displayed reduced fertility (Figures S1A–S1D), we focused on *rli2-1*/+ for further analysis.

Whereas wild-type siliques contained fully developed seeds, *rli2-1*/+ siliques contained ~14% white and wrinkled seeds and ~9% tiny and wrinkled ovules (Figures 1C–1E). Wild-type seeds contained heart-shaped embryo at 5 days after pollination, as revealed by whole-mount clearing (Figure 1J).[37,38] By contrast, the embryos in white *rli2-1*/+ seeds were arrested at the pre-globular stage and displayed abnormal cell division (Figure 1K). Because we did not obtain *rli2-1*/− mutant from self-fertilized *rli2-1*/+, it appears that the null mutation of *RLI2* causes embryonic lethality.[39] As *rli2-1*/+ siliques contained a few tiny and wrinkled ovules, it appears that the *RLI2* loss-of-function mutation also affected gametophyte development or fertilization. When we performed reciprocal crosses, the seed set was severely reduced when *rli2-1*/+ was used as the female parent and the wild type was used as the male parent (Figure 1F). By analyzing the progenies of different crosses, we determined that both the male and female gametophytic transmission ratios of *rli2-1* were severely reduced, suggesting that *RLI2* is critical for male and female gametophyte development (Table S1). Furthermore, wild-type embryo sacs developed normally during floral development stage 12c, as revealed by examining optical sections (Figure 1L), whereas some *rli2-1*/+ embryo sacs were abnormal, containing irregularly distributed nuclei (Figure 1M).

To confirm that the reduced fertility of the *rli2-1*/+ mutant was indeed caused by the loss of *RLI2* function, we performed complementation of *rli2-1*/+. We used the *RLI2* native promoter to drive *RLI2* genomic sequence fused with the *mCherry*-coding sequence and introduced this construct (*pRLI2*::*RLI2-mCherry*) into *rli2-1*/+. The exogenous *RLI2* fully complemented the reduced fertility and embryo lethal phenotypes of *rli2-1*/+ (Figures 1B, 1C, 1H, and 1I). These results suggest that the reduced fertility of *rli2-1*/+ was indeed due to lacking RLI2 function.

### RLI2 is essential for embryo and female gametophyte development

To determine at which stage *rli2-1*/+ seeds begin to show defects, we observed self-fertilized *rli2-1*/+ seeds by whole-mount clearing. We estimated the developmental stages of *rli2* embryos based on the stages of their wild-type siblings. After the first

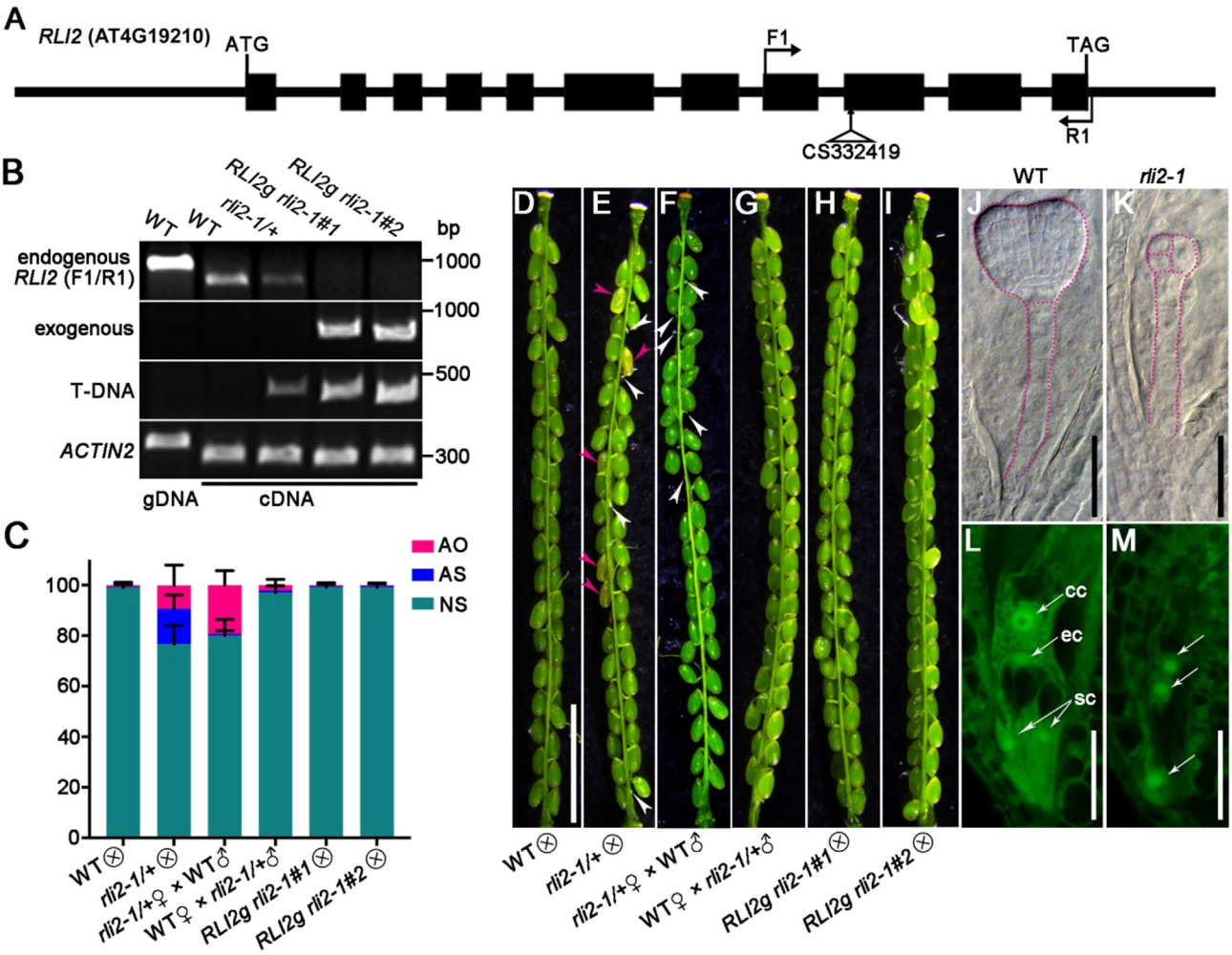


**Figure 1. Loss of function of *RLI2* has reduced fertility**

(A) Schematic diagram of the genomic region of *RLI2* and the transfer DNA insertion site of *rli2-1*. Boxes denote exons, lines represent untranslated regions or introns, and the triangle points to the transfer DNA insertion sites.

(B) Genotyping of *rli2-1*/+ and full-length *RLI2* gene complemented the *rli2-1*/− (*pRLI2*::*RLI2g-mcherry*+/+ *rli2-1*/−) plants; primers F1 and R1 are shown in (A). WT, wild type.

(C) Quantification of seed set for the designated genetic background. AO, aborted ovule; AS, aborted seed; NS, normal seed. Results shown are means ± SD ($n > 20$).

(D–I) Representative siliques from the different crosses. Pink arrowheads indicate aborted seeds, and white arrowheads indicate aborted ovules.

(J and K) Whole-mount clearing of WT (J) and *rli2-1* (K) embryos at 5 days after pollination. Dashed lines outline the developing embryos.

(L and M) Confocal laser scanning microscopy (CLSM) images of female gametophyte (FG) in WT (L) and *rli2-1* (M) at floral stage 13. cc, central cell; ec, egg cell; sc, synergid cell.

Scale bars, 2 mm (D–I) and 20 μm (J–M).

asymmetric zygotic division, ~13% of embryos from *rli2-1*/+ displayed abnormal cell division compared to wild-type embryos, as ~87% of *rli2-1*/+ embryos displayed similar cell division compared to wild-type embryos (Figures 2A and 2B). The cell-division patterns in these presumably *rli2* embryos continued to be impaired, leading to severe morphological defects and arrest at the globular stage (Figure 2B). In the arrested embryos, protoderm cells failed to form, abnormal divisions occurred in both the apical and basal lineages, and the embryonic surfaces were uneven (Figure 2B). By contrast, the *rli2* endosperm development was normal (Figures S1E and S1F). These results demonstrate that *RLI2* is essential for early embryonic pattern formation and cell division.

To determine how *RLI2* loss of function affects female fertility, we observed optical sections of *rli2-1*/+ ovules at different developmental stages by confocal laser scanning microscopy (CLSM).[40] In wild-type ovules, the functional megaspore (FM) adopted a teardrop shape, and the three degenerate megaspores became crushed at the micropylar end during stage 3-I (Figure 2C).[37,40] At this stage, the FM in *rli2-1* was comparable to that in the wild type (Figure 2D). Subsequently, the wild-type FM underwent three rounds of mitotic division and finally

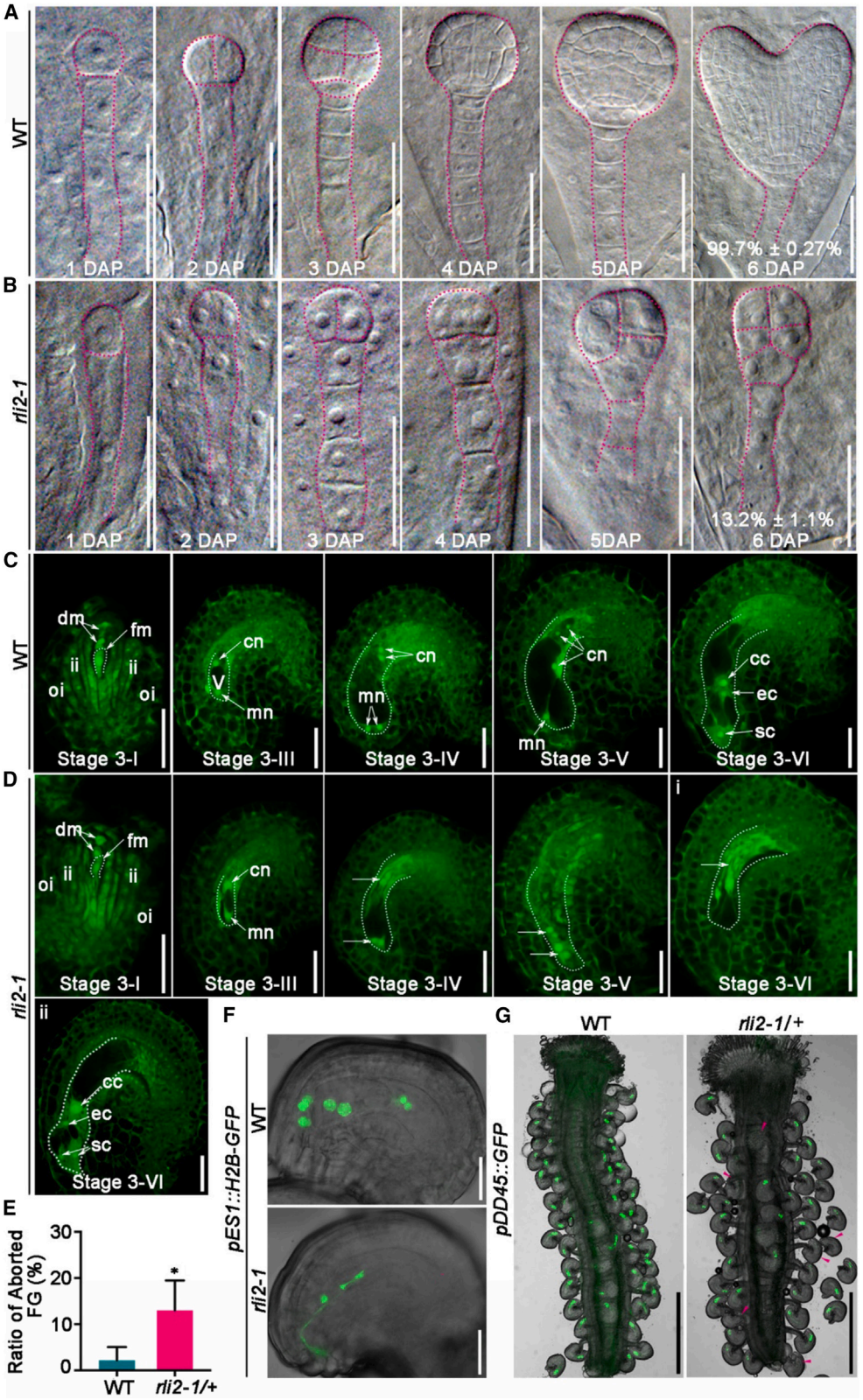


*(legend on next page)*

produced a mature embryo sac, which contained a central cell, an egg cell, and two synergid cells at stage 3-VI (Figure 2C). By contrast, although the nuclei in some embryo sacs of *rli2-1*/+ underwent mitosis beginning at the early stage, the division process, nuclei migration, and vacuole formation were affected during later stages, which led to almost 13% of *rli2-1*/+ embryo sacs collapsing at stage 3-VI (Figures 2Di and 2E). Meanwhile, the remaining *rli2-1*/+ FGs developed to mature embryo sacs (Figure 2Dii).

We then introduced *pES1*::*H2B-GFP*, in which nucleus-targeted GFP expression is driven by an embryo-sac-specific promoter, into *rli2-1*/+.[41] Eight nuclei were present in the wild-type embryo sac (Figure 2F), whereas 27 of 201 ovules from the *pES1*::*H2B-GFP rli2-1*/+ embryo sac contained a degraded GFP signal (Figure 2F). When we introduced the egg-cell reporter *pDD45*::*GFP* into *rli2-1*/+ to examine egg-cell differentiation,[42] some mature ovules in *rli2-1*/+ pistils did not show GFP signals in egg cells (Figure 2G). Interestingly, in addition to the degenerated embryo sac, the development of some *rli2-1*/+ embryo sacs was significantly delayed compared to the wild type (Figures S1G–S1J). When the wild-type embryo sacs developed into a mature 7-celled structure, the delayed *rli2-1*/+ embryo sacs had only 1–4 nuclei (Figures S1G–S1J), indicating that *RLI2* plays a critical role in female gametophyte development.

To further explore how *RLI2* affects embryo-sac development, we pollinated wild-type or *rli2-1*/+ pistils with pollen from *pLat52*::*GUS* plants (harboring a pollen-specific marker)[43] or wild type. We performed histochemical β-glucuronidase (GUS) staining or scanning electron microscopy (SEM) observation at 12 h after pollination. A GUS assay revealed that most wild-type ovules were targeted by one pollen tube (Figure S1K). By contrast, approximately 33% of ovules in *rli2-1*/+ failed to attract a pollen tube at this stage (Figure S1L). These ovules contained a pollen tube that exited the transmission track and grew along the funiculus but failed to enter the micropyle (Figures S1M and S1N). These results demonstrate that loss of function of *RLI2* causes embryo-sac abortion, leading to the failure of ovules to attract pollen tubes.

## Loss of function of *RLI2* impairs pollen tube germination

Under natural conditions *Arabidopsis* saturates pollination, as the number of pollen grains far exceeds the number of ovules. Therefore, when wild-type pistils are pollinated with heterozygous pollen, there is still enough wild-type pollen to complete the fertilization of all ovules. The seed set was comparable to that of the wild type when wild type was used as the female parent with *rli2-1*/+ as the male parent (Figures 1C and 1G). To determine how *RLI2* loss of function reduces the male transmission ratio (Table S1), we performed Alexander staining to analyze cytoplasmic viability, DAPI staining to examine the nuclear structure, and SEM to observe pollen morphology. All observations revealed that pollen development in *rli2-1*/+ was comparable to that in the wild type (Figures S2A–S2N and S2Q). Finally, we performed an *in vitro* pollen germination assay, finding that the pollen germination ratio was significantly lower in *rli2-1*/+ than in the wild type (Figures S2O, S2P, and S2R).

To further confirm that the *rli2-1* pollen germination was defective, we introduced the pollen tube marker *pLat52*::*GUS quartet1* (*qrt1*)[43,44] into *rli2-1*/+. Since the four pollen grains of *qrt1* remain fused during microsporogenesis, *qrt1* is usually used as a genetic tool to perform genetic analysis of a heterozygous plant, which makes it easy to distinguish the mutant pollen from wild-type pollen.[45] Wild-type pistils were hand-pollinated by a single tetrad from *pLat52*::*GUS qrt1* or *pLat52*::*GUS qrt1 rli2-1*/+ plants, and GUS-staining assay was performed after 24 h. We observed that at most four pollen tubes of one *qrt1* tetrad were guided to ovules, while at most three pollen tubes of one *rli2-1*/+ *qrt1* tetrad were guided to ovules (Figures S2S and S2U). Statistical analysis revealed that on average 2.1 pollen tubes were guided to ovules in one *qrt1* tetrad (four pollen grains could not separate and some pollen grains might not have touched stigma and germinated), while an average of 1.4 pollen tubes targeted ovules in one *rli2-1*/+ *qrt1* tetrad (Figure S2T). These results demonstrate that loss of function of *RLI2* causes defective pollen tube growth *in vivo*. Furthermore, more than two pollen tubes were guided to ovules in one *rli2-1*/+ *qrt1* tetrad (Figures S2S and S2U), indicating that the pollen germination ratio of *rli2-1*/+ exceeded 50% (Figures S2S and S2U). These results demonstrate that partial growth of *rli2-1* can guide pollen to ovules *in vivo*.

## *RLI2* is constitutively expressed in vegetative and reproductive organs, and RLI2 localizes to both the cytoplasm and nucleus

To examine the transcription patterns of *RLI2* in different plant tissues, we performed real-time qRT-PCR. *RLI2* was extensively expressed constitutively and was highly expressed in reproductive tissues such as inflorescence, ovule, pollen, and silique (Figure S3A), and we generated transgenic plants expressing *pRLI2*::*GUS*. Ten individual T2 generation transgenic plants exhibited similar GUS-staining signals in vegetative and reproductive tissues (Figures S3B–S3D). We also generated transgenic plants containing *pRLI2*::*H2B-GFP* and examined the expression of *RLI2* during reproductive growth. *RLI2* was consistently

**Figure 2. Loss of function of *RLI2* impairs embryo and FG development**

(A and B) Wild-type (WT) and *rli2-1* embryo development were visualized by differential interference contrast microscopy on different days after pollination (DAP). Dashed lines outline the embryo and division planes.

(C and D) CLSM images of ovules in WT (C) and *rli2-1*/+ (D) at different stages. (Di) The collapsed *rli2-1*/+ embryo sac at stage 3-VI. (Dii) The mature *rli2-1*/+ embryo sac at stage 3-VI. Dashed lines outline the functional megaspore at stage 3-I or the embryo sac at other stages, respectively. cc, central cell; cn, chalazal nucleus; dm, degenerating megaspore; ec, egg cell; fm, functional megaspore; ii, inner integument; oi, outer integument; mn, micropylar nucleus; sc, synergid cell; v, vacuole.

(E) Ratio of aborted FG based on CLSM of mature ovules in WT and *rli2-1*/+. Results shown are means ± SD ($n > 20$, t test, $p < 0.05$).

(F) Overlaid CLSM images from *pES1*::*H2B-GFP* and *pES1*::*H2B-GFP rli2-1*/+ transgenic plants.

(G) Representative pistils from *pDD45*::*GFP* and *pDD45*::*GFP rli2-1*/+ transgenic plants.

Scale bars, 20 μm (A–F) and 500 μm (G).

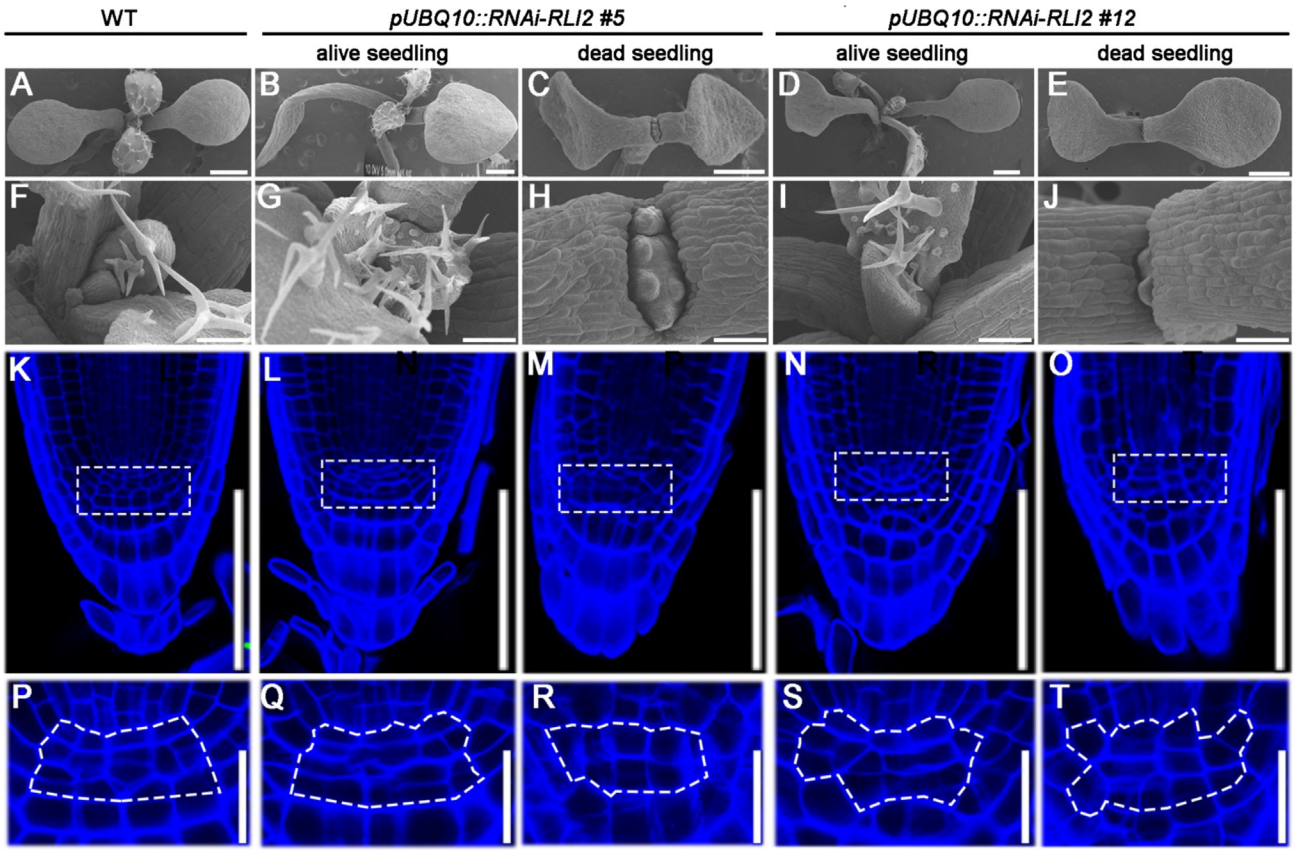


**Figure 3. *RLI2* knockdown mutant has abnormal root development and defective stem cell homeostasis**

(A–J) Scanning electron microscopy images of seedlings (A–E) and shoot apical meristem (SAM) regions (F–J) from wild type (WT; A, F), *pUBQ10*::*RNAi-RLI2 #5* (B, C, G, H), and *pUBQ10*::*RNAi-RLI2 #12* (D, E, I, J). The SAM regions in (A) to (E) are magnified in (F) to (J), respectively.

(K–T) Root tip architecture (K–O) and quiescent center (QC) organization (P–T) at 7 days after sowing the WT (K, P), *pUBQ10*::*RNAi-RLI2 #5* (L, M, Q, R), and *pUBQ10*::*RNAi-RLI2 #12* (N, O, S, T). The QC regions marked by dashed lines in (K) to (O) are magnified in panels (P) to (T), respectively. The progeny of *pUBQ10*::*RNAi-RLI2* lines showed developmental abnormalities with varying severity.

Scale bars, 500 μm (A–E), 100 μm (F–O), and 20 μm (P–T).

expressed at high levels in ovule, embryo, and pollen (Figures S3F–S3M). These tissue expression patterns revealed by *RLI2* promoter activity are consistent with the expression of *pRLI2*::*RLI2-mCherry* in *rli2-1* mutant (Figures S3N–S3U), indicating that *RLI2* is expressed in all tissues, especially reproductive tissues.

To examine the subcellular localization of RLI2, we introduced the *pRLI2*::*RLI2-GFP* vector into *rli2-1*/+ plant. GFP signals were detected in the cytoplasm and nuclei of root tip cells and pollen grains (Figures S3V and S3W), in agreement with results of the nucleocytoplasmic separation experiment (Figure S3X). These data reveal that RLI2 localized to both the cytoplasm and nucleus.

## Knockdown of *RLI2* causes multiple defects during *Arabidopsis* development

Because the embryonic-lethal/gametophyte-lethal phenotypes of the *RLI2* knockout mutant were too severe, we did not obtain a *rli2-1*/– mutant. To further provide support for the roles of *RLI2* in vegetative growth and reproductive development, we generated *RLI2* knockdown transgenic lines by expressing *pUBQ10*::*RNAi-RLI2* constructs specifically targeting *RLI2* driven by the constitutively expressed promoter *UBQ10*, which is also active in the embryo sac.[46] We identified ten T1 *RNAi-RLI2* lines that exhibited developmental abnormalities with varying severity and selected two lines (*#5*, *#12*) with the same developmental phenotypes for further analysis (Figures 3 and S4). In the progeny of these two transgenic lines, the phenotypes had segregated beginning in the T2 heterozygous (Figure S4A). Plants with the most severe phenotypes had flat cotyledons, abnormal shoot apical meristems (SAMs) and root apical meristems (RAMs), and disorganized quiescent centers (QCs). These plants died at the early seedling stage (Figures 3C, 3E, 3H, 3J, 3M, 3O, 3R, 3T, and S4B). Plants with moderate severe phenotypes had relatively normal SAMs and RAMs, but they died after the emergence of a few pairs of true leaves, and their rosette leaves were yellow and necrotic (Figures 3B, 3D, 3G, 3I, 3L, 3N, 3Q, 3S, S4C, and S4D). Although plants with less severe phenotypes survived and were propagated for several generations, the plants displayed defects in various tissues, such as smaller leaves, dwarfism, and reduced seed set (Figures S4E–S4I). These plants contained a

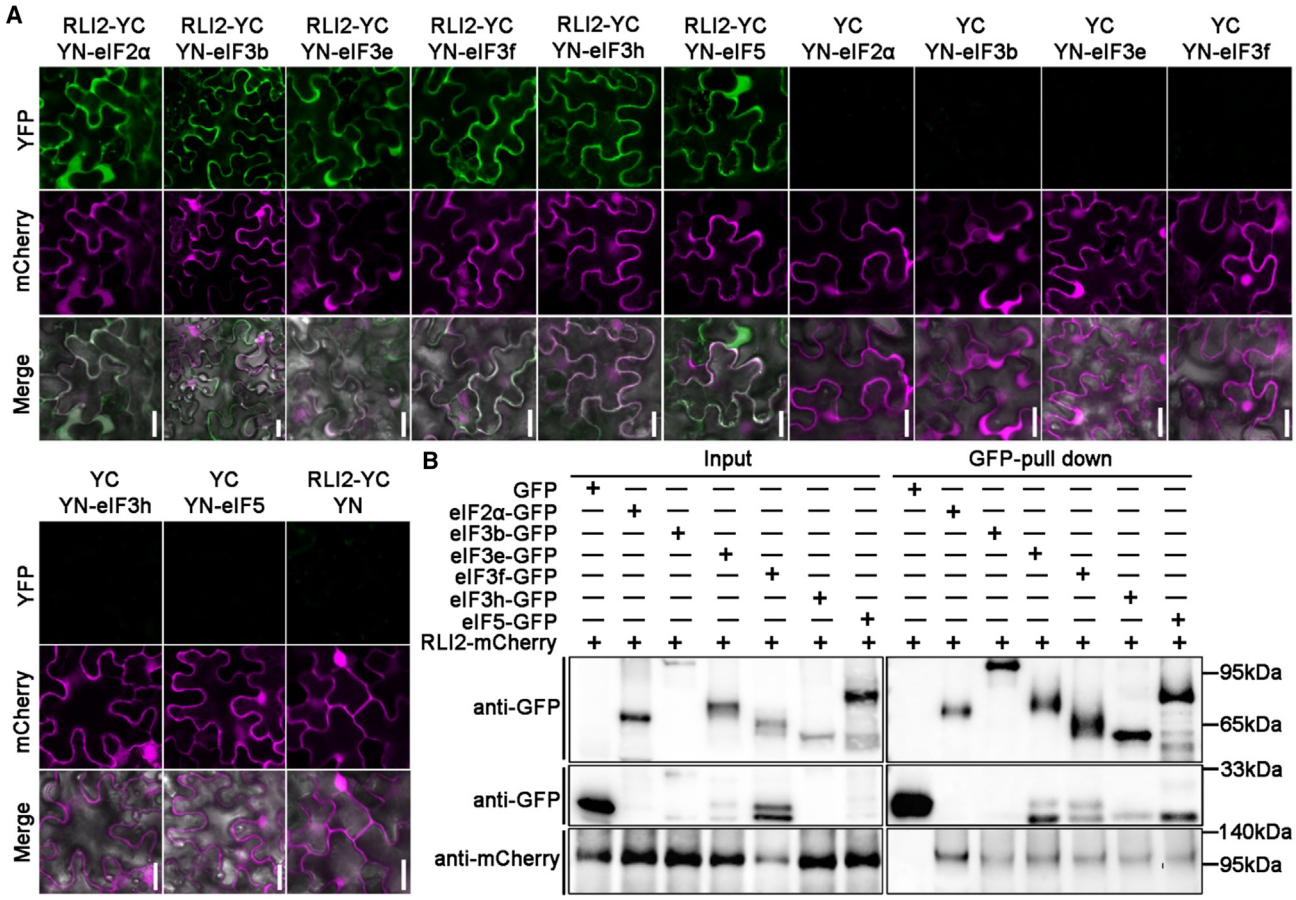


**Figure 4. RLI2 interacts with eIFs**

(A) BiFC experiments showed the interaction of RLI2-YC with YN-eIFs, including eIF2α, eIF3b, eIF3e, eIF3f, eIF3h, and eIF5.

(B) Co-immunoprecipitation (co-IP) experiments showed the interaction of RLI2-mCherry with GFP-tagged eIF2α, eIF3b, eIF3e, eIF3f, eIF3h, or eIF5. The indicated constructs were co-infiltrated in *N. benthamiana* leaves. Three independent experiments were performed for each combination with similar results. Scale bars, 20 μm.

high proportion of unfertilized ovules. When we examined these mature *RNAi-RLI2* ovules by CLSM, they displayed abnormal embryo sacs (Figures S4J–S4L). Consistent with the results obtained by CLSM, the ovules of *pES1*::*H2B-GFP RNAi-RLI2* plants exhibited only one nucleus or a degraded embryo sac (Figures S4M–S4O). These results demonstrate that the reduced seed set in *RNAi-RLI2* plants is partially due to embryo-sac abortion (Figures S4P and S4Q).

Correspondingly, qRT-PCR results indicated that *RLI2* transcription levels were lower in *RNAi-RLI2* than in wild-type plants, which were strongly associated with plant phenotypes (plants with lowest *RLI2* transcriptions have most severe phenotypes) (Figures S4R and S4S). This is further supported by the dramatically reduced expression levels of RLI2-mCherry fusion protein in *RNAi-RLI2* plants (Figure S4T). Moreover, the transcription levels of *RLI1* (AT3G13640), the homolog gene of *RLI2*, was not influenced in *RNAi-RLI2* plants (Figure S4U), suggesting the specific downregulation of *RLI2*. These results demonstrate that the knockdown of *RLI2* causes pleiotropic developmental defects in *Arabidopsis*.

## Phylogenetic analysis of *RLI* genes

To further investigate the regulatory mechanism of RLI2 functions in regulating plant growth and development, we compared the amino acid sequence of AtRLI2 with the sequences of RLI/ABCE from other species, including eukaryotes and prokaryotes, using data from the National Center for Biotechnology Information (NCBI) (https://blast.ncbi.nlm.nih.gov/Blast.cgi). Protein sequence alignment revealed that the full sequences of RLI/ABCE in different plants are highly conserved (Figure S5A). Phylogenetic analysis indicated that AtRLI2 shares 97.7% identity with homologs in *Brassica napus* (GenBank: XP_013678613) and 86%–92% identity with homologs in dicots and monocots, such as tobacco (*Nicotiana attenuata*, GenBank: XP_019231970), tomato (*Solanum lycopersicum*, GenBank: XP_004246016), alfalfa (*Medicago truncatula*, GenBank: XP_013466185), rice (*Oryza sativa Japonica*, GenBank: XP_015617612), and barley (*Hordeum vulgare*, GenBank: KAE8790295) (Figure S5B). Furthermore, AtRLI2 shares 59%–85% identity with its putative orthologs in animals, such as human (*Homo sapiens*), mouse (*Mus musculus*), fruit fly (*D. melanogaster*), and nematode (*C. elegans*) (Figure S5B). AtRLI2 also shares

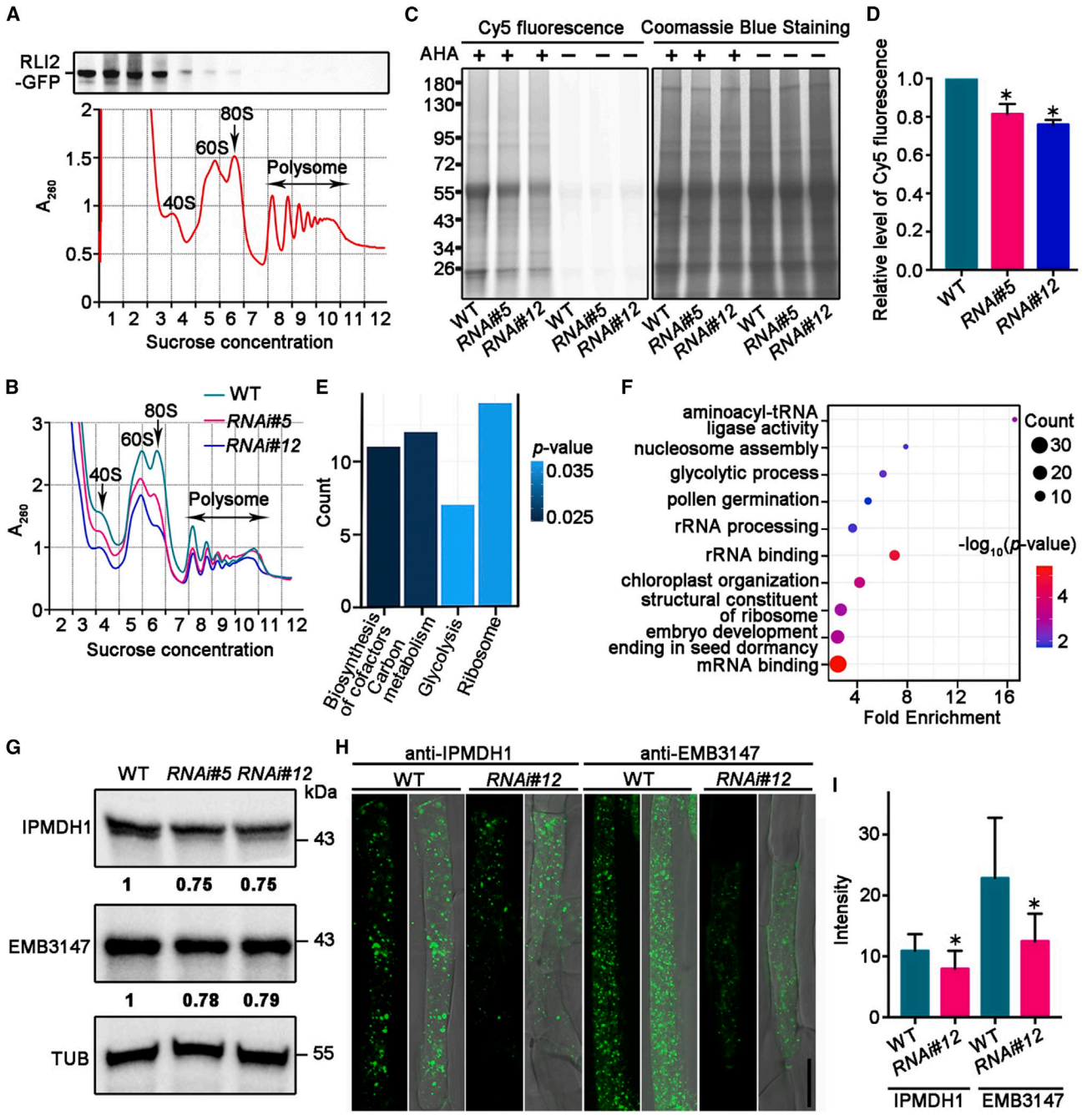


**Figure 5. Knockdown of *RLI2* reduces ribosomal biogenesis and translational efficiency**

(A) Analysis of the RLI2 protein in polysome profiling fractions. *pRLI2*::*RLI2-GFP rli2-1*/− transgenic plants were used for polysome profile assay by sucrose density gradients, which were collected with continuous scanning at 260 nm. Three independent experiments were conducted with similar results.

(B) Analysis of polysome profiles in wild type (WT), *pUBQ10*::*RNAi-RLI2 #5*, and *#12*. The 40S, 60S, and 80S ribosome peaks are indicated. The experiment was repeated three times with similar results.

(C) SDS-PAGE images of protein synthesis by azide labeling.

(D) Qualification of the relative levels of Cy5 fluorescence signal. Data represent means ± SD of three independent experiments. Asterisks indicate a significant difference (t test, $p < 0.05$).

(E) KEGG pathway analysis of downregulated genes (*pUBQ10*::*RNAi-RLI2 #12* versus WT) in proteome analysis.

(F) GO analysis of downregulated genes (*pUBQ10*::*RNAi-RLI2 #12* versus WT) in proteome analysis.

*(legend continued on next page)*

40%–68% identity with its putative orthologs in bacteria and fungi, such as archaea (*Pyrococcus abyssi*) and yeast (*Saccharomyces cerevisiae*) (Figure S5B). Interestingly, the RLI/ABCE family consists of two members in some species, suggesting that *RLI/ABCE* gene duplication occurred during evolution (Figure S5B). To investigate whether the *RLI*s in animals and fungi also function in plants, we introduced *MmRLI1* (GenBank: NP_056566) and *ScRLI1* (YDR091C) to *rli2-1*/+ plants driven by the promoter of *Arabidopsis RLI2*. The results showed that the seed set of *pRLI2*::*MmRLI1* and *pRLI2*::*ScRLI1* transgenic plants in *rli2-1*/+ background did not show a significant difference from *rli2-1*/+ mutant (Figures S5C and S5D), indicating that the *RLI* genes from *M. musculus* and *S. cerevisiae* could not restore the *rli2-1*/+ phenotype. We also performed complementation experiments in yeast with two *Arabidopsis RLI* genes. Since loss of function of yeast *ScRLI1* gene leads to lethality,[9] we transformed the plasmid containing *ScRLI1* gene into yeast before knocking out *ScRLI1* gene in the yeast genome. We then introduced *AtRLI1* and *AtRLI2* to *ScRLI1*-depleted yeast separately to investigate whether *Arabidopsis RLI* genes could replace the function of *ScRLI1* gene (Figures S5E and S5F). The results revealed that the exogenous *AtRLI1* and *AtRLI2* could not rescue the lethal phenotype while *ScRLI1* could rescue it (Figure S5F), suggesting that *AtRLI*s could not replace the function of *ScRLI1*. Collectively, these results suggest that *Arabidopsis RLI* genes and *ScRLI1* gene could not replace each other.

## Knockdown of *RLI2* affects the assembly of the translational machinery

The RLI/ABCE protein subfamily is the most evolutionarily conserved group of ABC proteins. The biological functions of RLI/ABCE subfamily members are also highly conserved in different species.[14] It was reported that RLI participates in multiple translation processes, including ribosome biogenesis, recycling, and reactivation, and translation initiation.[9] We therefore reasoned that *Arabidopsis* RLI2 plays a role in translation.

In yeast, ScRLI1 is associated with eIF2$\alpha$ (SUI2), eIF3 subunits (eIF3b/PRT1, eIF3g/TIF35, eIF3j/HCR1), and eIF5/TIF5.[9] However, the roles of eIFs in plants are largely unknown. To determine whether RLI2 associates with eIF homologs in *Arabidopsis*, we performed bimolecular fluorescence complementation (BiFC) assays. *Arabidopsis* contains two homologs of *eIF2*$\alpha$.[47] We selected one of these genes (AT5G05470) for analysis because it encodes a protein that localizes to the cytoplasm according to gene ontology (GO) analysis of cellular components, while another gene is expressed in the nucleus, chloroplast, and Golgi apparatus. Because the eIF3 complex in *Arabidopsis* consists of 11 members,[48] we selected the previously reported eIF3 subunits eIF3b/AT5G25780, eIF3e/AT3G57290, eIF3f/AT2G39990, and eIF3h/AT1G10840 for further study. Although the function of eIF5 has not been reported, one putative candidate *Arabidopsis*, *eIF5* (AT1G77840) was identified in GenBank. Among these eIFs, eIF2$\alpha$, eIF3b, eIF3e, eIF3f, eIF3h, and eIF5 interacted with RLI2 in the cytoplasm in a BiFC assay (Figure 4A). We further verified their interactions with RLI2 by co-immunoprecipitation (co-IP) assays (Figure 4B). In addition, more investigations revealed that RLI2 is also associated with other ribosome formation and biogenesis factors (RPL23aB/AT3G55280 and RPS2B/AT1G58684) and release factors (ERF1-1/AT5G47880, ERF1-2/AT1G12920, ERF1-3/AT3G26618, and EF1$\alpha$/AT1G18070) revealed by BiFC and co-IP assays (Figure S6), suggesting that RLI2 is involved in multiple translation processes.

To further verify that RLI2 interacts with translation factors and associates with the translation apparatus, we analyzed RLI2 protein of all sample fractions collected from the polysome profiling through western blot analysis. The results revealed that RLI2 protein appears in 40S, 60S, and 80S ribosome fractions but not in the polysome fractions (Figure 5A), indicating that RLI2 was associated with the ribosome. To evaluate the effect of knocking down *RLI2* on ribosome assembly, we performed polysome profiling of *RNAi-RLI2* plants and observed an obvious reduction in the abundance of 40S, 60S and 80S ribosomal subunits compared to the wild type (Figure 5B). Thus, knockdown of *RLI2* impaired ribosome assembly. These results suggest that RLI2 likely interacts with the translation-related factors to participate in the assembly of the translational machinery.

## Knockdown of *RLI2* affects translational efficiency

The reduced ribosome abundance of *RNAi-RLI2* plants suggests that RLI2 might be involved in controlling translational efficiency. To further confirm the role of RLI2 in regulating translational efficiency, we examined the relative levels of newborn proteins in wild-type and *RNAi-RLI2* plants using L-azidohomoalanine (Click-iT AHA) labeling, which reacts with Cy5. The results showed that the relative levels of Cy5 fluorescence in *RNAi-RLI2* plants were significantly reduced compared to those of the wild type (Figures 5C and 5D), suggesting that the abundance of azide-modified proteins marking the newborn proteins in *RNAi-RLI2* plants was significantly reduced. These data suggest that knocking down *RLI2* caused reduced translational efficiency. To identify proteins with altered abundance due to impaired RLI2 function in *RNAi-RLI2* plants, we performed proteome analysis of wild-type and *RNAi-RLI2 #12* seedlings via 4D-label-free proteomics. We obtained 30,331 peptides and identified 5,650 proteins in all samples (Figures S7A–S7C). High data reproducibility was observed for both the wild type and *RNAi-RLI2* (Figure S7D). In addition, 335 proteins (113 upregulated proteins and 222 downregulated proteins) showed altered abundance in *RNAi-RLI2* compared to Columbia-0 (Col-0) (fold change $\geq$ 2 and $p < 0.05$); 205 proteins were only identified twice from a set of samples (121 upregulated proteins and 94 downregulated proteins) (Figure S7B and Data S1).

Kyoto Encyclopedia of Genes and Genomes (KEGG) analysis of translationally downregulated genes in the *RNAi-RLI2* line revealed enrichment in the ribosome (ath03010), glycolysis (ath00010), carbon metabolism (ath01200), and biosynthesis of cofactors (ath01240) pathways ($p < 0.05$) (Figure 5E), whereas

(G and H) Western blot (G) and immunofluorescence (H) analysis of the levels of IPMDH1 (AT5G14200) and EMB3147 (AT2G30200) proteins using anti-IPMDH1 and aniti-EMB3147 in WT and *pUBQ10*::*RNAi-RLI2 #12*. Scale bar, 20 $\mu$m.

(I) GFP intensity in the cells from immunofluorescence in (H) in WT and *pUBQ10*::*RNAi-RLI2 #12*. The results shown are means $\pm$ SD ($n > 15$). Asterisks indicate a significant difference (t test, $p < 0.01$).

there was no enrichment in any specific biological process for the upregulated genes. GO analysis of translationally downregulated genes in *RNAi-RLI2* revealed enrichment in the GO terms including mRNA binding (GO:0003729), structural constituent of ribosome (GO:0003735), rRNA binding (GO:0019843), rRNA processing (GO:0006364), and aminoacyl-tRNA ligase activity (GO:0004812), which are related to translation; and embryo development ending in seed dormancy (GO:0009793), pollen germination (GO:0009846), glycolytic process (GO:0006096), chloroplast organization (GO:0009658), and nucleosome assembly (GO:0006334), which are related to fundamental aspects of plant growth (Figure 5F). GO analysis of translationally upregulated genes in *RNAi-RLI2* revealed enrichment in stress-related GO terms (Figure S7E). To demonstrate whether these translationally affected proteins were differentially regulated at the transcription level, we performed RNA-seq. Few genes were differentially expressed in both the proteome and RNA-seq data, indicating that genes encoding proteins with reduced abundance in the *RNAi-RLI2* line were indeed differentially regulated in this line versus Col-0 at the translational level (Figure S7F).

We suspected that the pleiotropic developmental defects of the *RNAi-RLI2* mutants could result from a general decrease in the translation levels of some important proteins. To test this possibility, we monitored the levels of ISOPROPYLMALATE DEHYDROGENASE 1 (IPMDH1) and EMBRYO DEFECTIVE 3147 (EMB3147) proteins by western blot and immunofluorescence using anti-IPMDH1 and anti-EMB3147 antibodies, respectively, based on the proteome data. Their protein levels were reduced in *RNAi-RLI2* (Figure 5G), which is in agreement with the obviously decreased immunofluorescence signals in the root epidermis cells of the maturation zone (Figures 5H and 5I). Mutants of these proteins exhibit defects in different developmental processes. For example, *emb3147* mutant shows embryo lethality,[49] similar to the *RLI2* transfer DNA mutant. *ipmdh1* mutant displays smaller leaves than the wild type,[50] like the *RLI2* knockdown plant. These results suggest that *RLI2* knockdown results in reduced translational efficiency.

## Knockdown of *RLI2* disturbs auxin homeostasis

To gain further insight into the function and regulation of *RLI2* in plant development, we analyzed the transcriptional changes in Col-0 and *RNAi-RLI2 #12* seedlings by RNA-seq. We obtained an average of ~50 million clean reads from each sample and identified 3,255 genes (1,778 upregulated genes and 1,477 downregulated genes) with altered expression levels in *RNAi-RLI2* compared to Col-0 ($\log_2$ fold change $\geq$ 1.0 and false discovery rate < 0.05) (Figure S8A and Data S2). KEGG pathway analysis revealed that the basal metabolism pathway, especially biosynthesis of amino acids and secondary metabolites and metabolism of starch and sucrose, were greatly enriched among the differentially expressed genes (DEGs) (Figure S8B). Moreover, essential signaling pathways, such as plant hormone signal transduction, MAPK signaling pathway, plant-pathogen interaction, and circadian rhythm were also greatly enriched in *RNAi-RLI2* seedlings (Figure S8B). These results suggest that RLI2 functions in multiple processes.

We performed GO enrichment analysis to identify phytohormone-related genes among the DEGs. The DEGs showed significant enrichment in the GO terms, including hormone metabolic process (GO:0042445), hormone biosynthetic process (GO:0042446), hormone transport (GO:0009914), response to hormone (GO:0009725), cellular response to hormone stimulus (GO:0032870), hormone-mediated signaling pathway (GO:0009755), and regulation of hormone levels (GO:0010817) (Figure S8C). To identify which phytohormone signaling pathways were disturbed in *RNAi-RLI2* seedlings, we performed GO enrichment analysis of the biological processes of different phytohormones among the upregulated and downregulated DEGs (Figures S8D and S8E). Auxin-related terms, such as auxin biosynthetic process (GO:0009851), auxin transport (GO:0060918), and response to auxin (GO:0009733), were strongly enriched among the downregulated genes but not the upregulated genes (Figure S8E). These data suggest that RLI2 affects the auxin signaling pathway.

Auxin plays a prominent role in embryo development and is the only phytohormone that is maintained at high levels from fertilization to seed maturation.[51,52] We therefore examined the expression of the auxin response reporter *DR5*::*V2-GFP* in the wild type. The apical cell lineage showed DR5 reporter activity in zygotes after cell division, followed by restricted DR5 expression in the hypophysis at the globular stage (Figure 6A). New DR5 maxima appeared at the flanks of the apical embryo during the transition stage, as previously reported.[53] By contrast, DR5 signals failed to establish an apical-basal gradient in some *DR5*::*V2-GFP rli2-1*/+ embryos at the 8-cell stage, while were restricted to the basal cell lineage at the globular stage (Figure 6B). These results suggest that RLI2 regulates auxin distribution during apical-basal patterning in early embryogenesis.

Further evidence for the impaired auxin signaling pathway in *RNAi-RLI2* plants came from the proteome data that illustrated the reduced protein level of the transcriptional activator MONOPTEROS (MP)/AUXIN-RESPONSIVE FACTOR 5 (ARF5), which is a critical regulator for embryo and seedling development.[54] RNA-seq data and qRT-PCR results showed that the transcription levels of *MP* were unchanged in *RNAi-RLI2* plants (Figure S9C), excluding the influence of transcriptional regulation. We then introduced a construct, *pMP*::*MP-GFP*, into *RNAi-RLI2* plants. MP-GFP signals and protein levels were significantly reduced in *RNAi-RLI2* compared to the wild type (Figures 6C–6H). These results suggest that RLI2 regulates the translational efficiency of MP to influence auxin homeostasis.

The polar auxin transport protein PIN-FORMED7 (PIN7) regulates embryo and seedling development.[53] We therefore introduced *pPIN7*::*PIN7-GFP* into *RNAi-RLI2* plants. The transcription levels of *PIN7* were unchanged in *RNAi-RLI2* plants (Figure S9D), indicating the influence mainly in translation regulation. By contrast, PIN7-GFP signals and protein levels were significantly reduced in *RNAi-RLI2* compared to the wild type (Figures S9E–S9J). These results suggest that RLI2 also regulates the translational efficiency of PIN7 to influence polar auxin transport, although PIN7 was not detected by proteomics. Therefore, the regulation of translational efficiency is important for many key regulators of auxin.

Finally, genes associated with resistance-related plant hormones, such as jasmonic acid, salicylic acid (SA), and abscisic acid (ABA), were enriched among upregulated genes in *RNAi-RLI2* versus Col-0 (Figure S8D). These results demonstrate that the knockdown of *RLI2* disturbs phytohormone homeostasis in *Arabidopsis*.

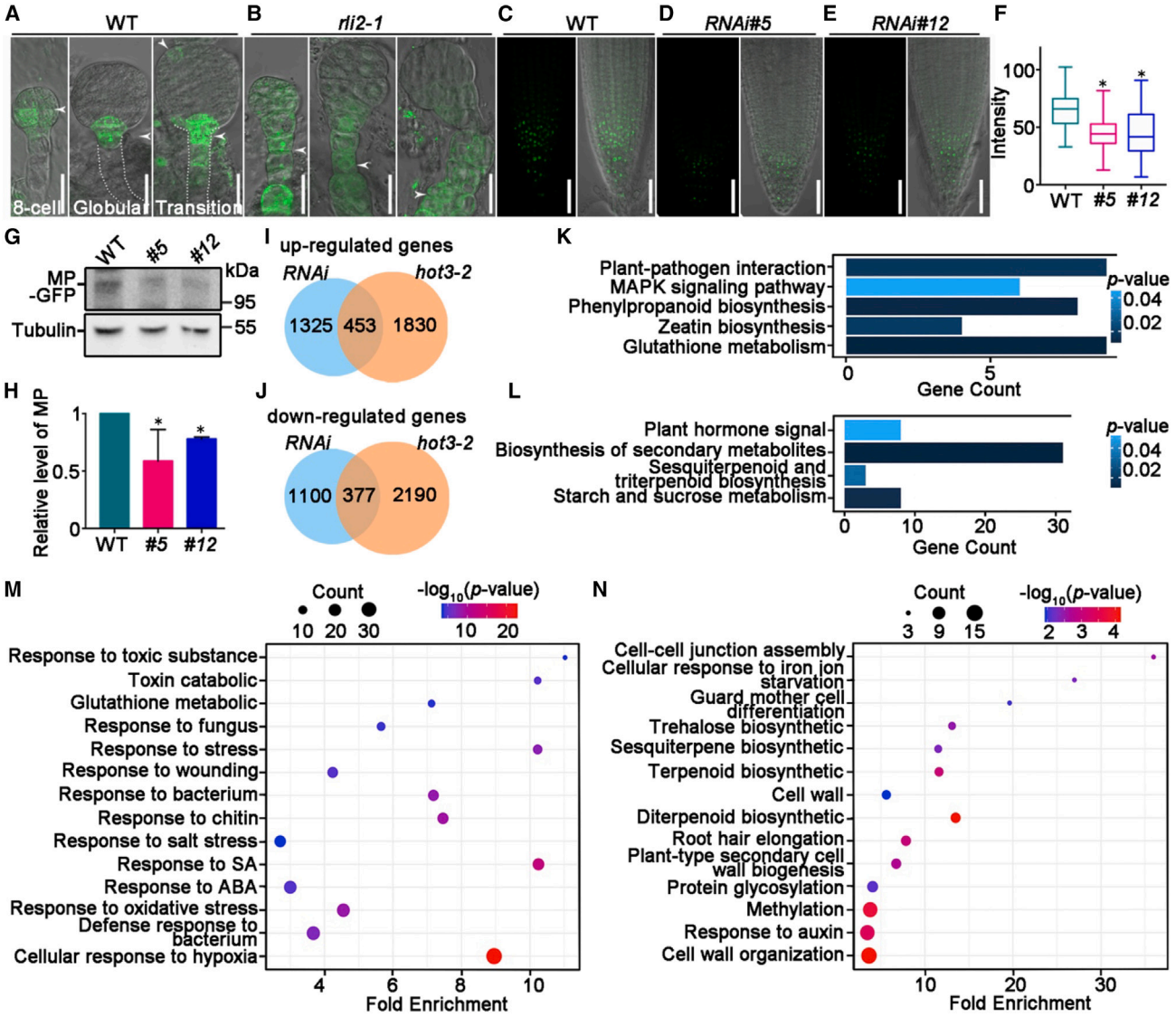


**Figure 6. The auxin homeostasis is disturbed in *RLI2* mutants**

(A and B) *DR5*::*GFP* in wild-type (WT) and *rli2-1* embryos at different stages. Arrowheads point to cells with auxin response maximum.

(C–E) *pMP*::*MP-GFP* (C) and *pMP*::*MP-GFP pUBQ10*::*RNAi-RLI2 #5* (D) and *#12* (E) in root tips. The GFP channel and transmission channel are merged in the right-hand panels.

(F) GFP intensity in the nucleus for MP-GFP from *pMP*::*MP-GFP*, and *pMP*::*MP-GFP pUBQ10*::*RNAi-RLI2 #5* and *#12*. The results shown are means ± SD ($n > 28$). Asterisks indicate a significant difference (t test, $p < 0.01$).

(G and H) Western blot detection of MP-GFP protein abundance in *RNAi-RLI2* plants (G), and quantification of the relative levels of MP-GFP protein (H). Data are means ± SD. Asterisks indicate a significant difference (t test, $p < 0.05$).

(I and J) Venn diagrams show the upregulated genes (I) and downregulated genes (J) that overlap between the *RLI2* knockdown mutant and *hot3-2* mutant.

(K and L) KEGG pathway analysis of overlapping genes upregulated (K) and downregulated (L) in both the *RLI2* knockdown mutant and *hot3-2* mutant.

(M and N) GO analysis of overlapping genes upregulated (M) and downregulated (N) in both *RLI2* knockdown mutant and *hot3-2* mutant.

Scale bars, 20 μm (A and B) and 50 μm (C and D).

## Genes involved in the auxin signaling pathway are differentially expressed in both *RLI2* knockdown and *hot3-2* mutants

To gain further insights into the role of RLI2 in translational regulation, we analyzed genes that were differentially expressed in both *RNAi-RLI2* and the *eIF5B* mutant *hot3-2* compared to Col-0.[55] These genes showed significant overlap (Figures 6I and 6J; Data S3). KEGG analysis revealed that the 453 overlapping upregulated genes were strongly enriched in pathways related to plant-pathogen interactions, MAPK signaling, and metabolism (Figure 6K). The 377 overlapping downregulated genes were strongly enriched in pathways related to plant hormone signal transduction and metabolism (Figure 6L). GO analysis (biological process) revealed that these DEGs were also

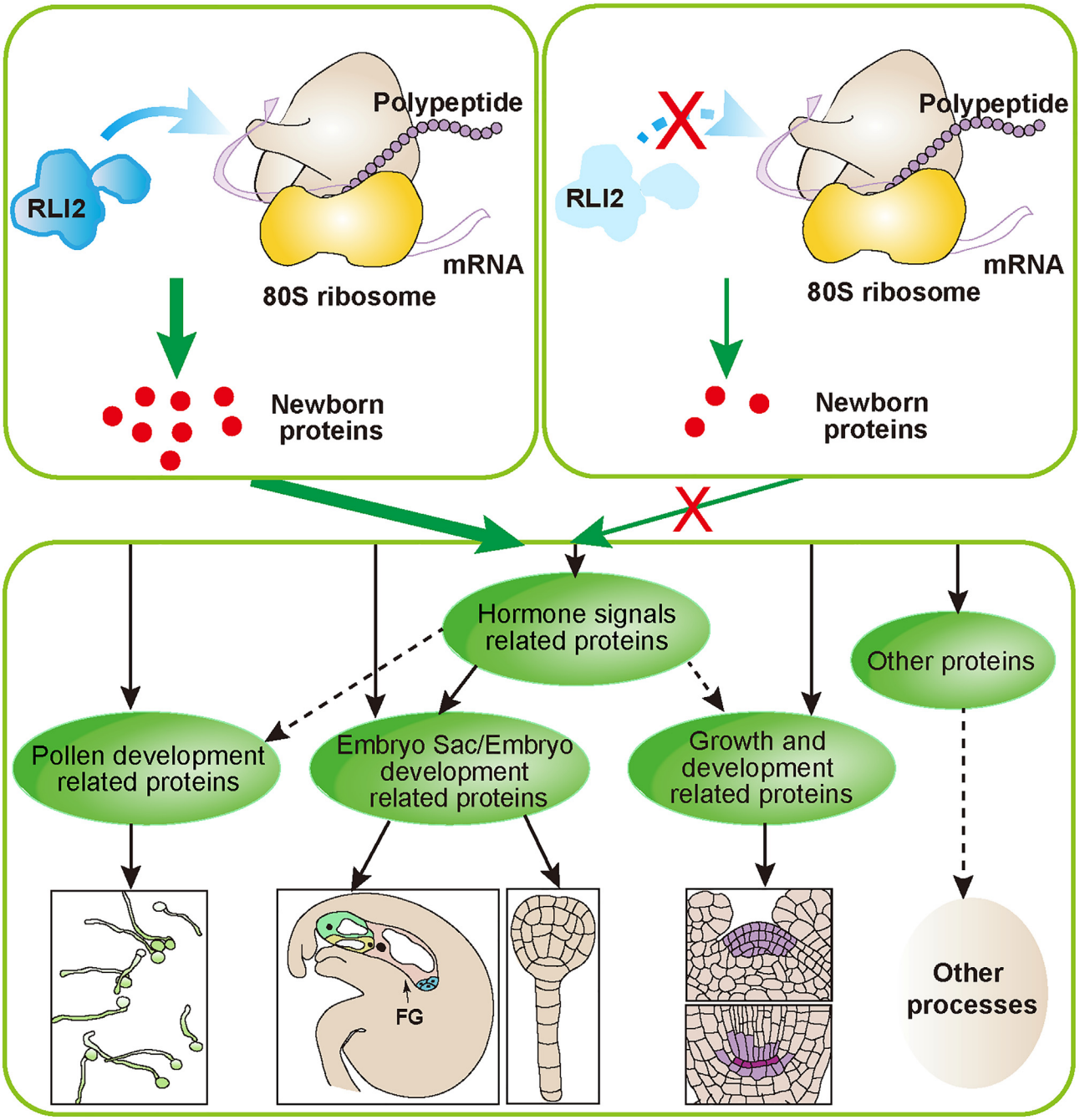


**Figure 7. Work model of RLI2 participates in translational machinery and regulates plant development**

RLI2 interacts with several translation-related factors (ribosome formation and biogenesis related factors, eIFs, and release factors) to become involved in assembling translational machinery. RLI2 may regulate the translational efficiency of multiple proteins involved in growth and development, hormone signals, and other processes which are critical for pollen development, embryo-sac/embryo development, and so forth.

enriched in stress-related and hormone-related terms (Figure 6M). Importantly, the upregulated genes were strongly enriched in SA- and ABA-related terms (Figure 6M), and the downregulated genes were strongly enriched in auxin-related terms (Figure 6N). This overlap of DEGs in phytohormone signal transduction in both *RNAi-RLI2* and *hot3-2* suggests that RLI2 and eIF have similar functions in plant hormone homeostasis. These results suggest that RLI2 interacts with eIFs to regulate downstream phytohormone signaling, especially auxin signaling, to positively regulate plant growth.

## DISCUSSION

In this study, we identified RLI2 as a new player in the translational machinery in *Arabidopsis*. We proposed that RLI2 interacts with eIFs, ribosome formation and biogenesis factors, and translation release factors to participate in the assembly of the translational machinery to regulate plant growth and development (Figure 7). Several lines of evidence supported this notion. First, a null mutation of *RLI2* was gametophytic- and embryonic-lethal (Figures 1 and 2), whereas the knockdown of *RLI2* caused pleiotropic defects (Figure 3), a common phenotype of translation-related mutants.[55–57] Second, RLI2 physically interacted with multiple translation-related factors. Third, knocking down *RLI2* obviously decreased the abundance of 40S, 60S, and 80S ribosomal monomers and polysomes. Finally, proteome analysis determined that knockdown of *RLI2* resulted in the altered translational efficiency of proteins, especially ribosomal proteins.

Because 50% of *rli2*/+ pollens are wild-type pollens with normal development and *Arabidopsis* saturates pollination under natural conditions, the normal pollen will compete with the *rli2-1* mutant pollen during fertilization, resulting in a significantly reduced transmission ratio of *rli2-1* pollen. The low transmission ratio of *rli2-1* pollen did not influence the seed set in *rli2-1*/+. Besides, the reduction of seed set was mainly caused by the abnormal development of the *rli2-1* embryo sac and embryo. Further investigations revealed that part of *rli2-1* pollen grains can germinate on the stigma and be guided to the ovule, which is supported by *pLat52*::*GUS* activity in *rli2-1*/+ plants. In addition, knockdown of *RLI2* leads to defective vegetative growth, indicating that RLI2 influences pollen and functions in the other process of plant growth and development.

In *Arabidopsis*, the RLI family consists of two members. qRT-PCR showed that *RLI1* is mainly expressed in reproductive tissues, which is similar to *RLI2* (Figure S3E). However, the transcription level of *RLI1* is significantly lower than that of *RLI2*, suggesting that *RLI1* may not play predominant roles in plant growth and development.

The most widely studied function of ABCE/RLI is its involvement in translation processes. We cannot rule out the possibility that ABCE/RLI plays a role in every translation stage in every species. A study based on cryo-electron microscopy reconstruction of the late-stage 48S initiation complex from rabbit suggested that ABCE1 is a bona fide initiation factor throughout the entire initiation phase. ABCE1 is also a multi-tasking factor that functions in coordinated termination, recycling, and initiation.[10] Pixie, an ABCE/RLI homolog in *Drosophila*, is required for normal translation and ribosomal recycling.[7,20] In yeast, ScRLI1 functions in translation initiation, translation termination, ribosome biogenesis, and ribosome recycling.[9,58,59,60] In *C. elegans*, ABCE protein interacts with both the cytoplasmic protein RPL-4 and the nuclear protein NHR-91, suggesting that ABCE might be involved in controlling translation and transcription, function as a shuttle protein between the cytoplasm and nucleus, and possibly function as a nucleocytoplasmic transporter.[21] Knockout of *ABCE1* altered the abundance of polysomes and 80S ribosomal monomers in yeast, *Drosophila*, and mammals.[14] Here we showed that knocking down *RLI2* resulted in the decreased abundance of 40S, 60S, and 80S ribosomal monomers (Figure 5B). Protein interaction results revealed that RLI2 interacts with eIFs, ribosome formation, biogenesis factors (RPL23aB and RPS2B), and release factors (ERF1-1, ERF1-2, ERF1-3, and EF1$\alpha$) to function in multiple translation processes, thus affecting the translational efficiency in *Arabidopsis* (Figures 4, 5, and S6). Our results suggested that *Arabidopsis RLI* genes and yeast *ScRLI1* gene could not replace each other (Figures S5E and S5F), implying that they may be involved in different translation processes.

In addition to participating in the translation process, ABCE proteins act as endogenous suppressors of RNA silencing in plants and humans.[18,61] ABCE1 not only forms a heterodimer specifically with RNase L to non-competitively inhibit its binding to 2-5A,[19] but is also involved in histone biosynthesis and DNA replication in humans.[62] Accordingly, we speculate that RLI2 may regulate gene expression in different manners. To further investigate how ABCE/RLI regulates plant developmentcs analysis (Figures 5 and 6). Proteomics analysis illustrated that embryo-related and pollen-germination-related proteins were enriched among the proteins with differential abundance in wild type and *RNAi-RLI2*, suggesting that RLI2 affects the translational efficiency of these proteins to regulate embryo development and pollen germination (Figure 5).

Transcriptomic analysis revealed that genes related to the auxin signaling pathway were significantly downregulated in *RNAi-RLI2* plants compared to the wild type. Further enrichment analysis of downregulated genes in both *RNAi-RLI2* plants and *hot3-2* mutant revealed that auxin signaling was significantly inhibited in both lines; the transcription levels of auxin-related genes were suppressed to varying degrees in both lines (Figure 6). Both the *rli2-1* and *eif3h-1* mutants were shown to have altered auxin responses.[63] These findings suggested that inhibited auxin signaling is a common feature of mutants with impaired translational machinery and that the developmental defects caused by impaired translation are in part due to defects in auxin signaling.

Because of the sensitivity of proteome and spatiotemporal expression of different proteins, and the knockdown expression of *RLI2* in *RNAi-RLI2* plants, we cannot detect all RLI2 target proteins in proteome analysis, so we cannot exclude the possibility that RLI2 shows no preference or specificity for the translation of proteins. Since knockdown of *RLI2* leads to pleiotropic defects of plant growth and reproductive development and RLI2 interacts with multiple translation-related factors, we speculate that RLI2 regulates the basic translational process, which is critical for multiple processes of development.

Based on our proteome and RNA-seq data, we also isolated other genes involving in *Arabidopsis* growth and development. *Arabidopsis ankyrin repeat protein* (*AKRP*),[64] *acetoacetyl-CoA thiolase 2* (*AACT2*),[65] and *non-intrinsic ABC protein 7* (*ATNAP7*)[66] are essential for gametophyte and embryo development. *ABCB19* regulates embryo, root, and hypocotyl elongation by involving in auxin transport.[67] *CADMIUM$^{2+}$ INDUCED* (*CDI*),[68] *FIMBRIN5*,[69] and *AtGT11*[70] are required for pollen germination and tube growth. Chloroplast-localized *RNASE E* is required for vegetative growth.[71] The data indicated that RLI2 possibly regulated the translational efficiency of multiple proteins in a general rather than specific manner. The reduced abundance of the aforementioned proteins may contribute to the corresponding developmental defects in the *RLI2* mutant.

Mutations in genes encoding ribosome-related proteins commonly influence ribosome biogenesis, resulting in gametophytic lethality due to the compromised mitotic cell-cycle progression during gametophyte development.[28,30–36] Loss of function of *RLI2* also triggered embryo defect (Figure 2B), suggesting that RLI2 may have extra functions beyond the aforementioned ribosome-related proteins. AtRPL10 has functions and localization patterns similar to those of RLI2 (Figures S3V–S3X),[72] indicating that RLI2 extra functions are possibly connected to its localization. Moreover, the defective embryos in *rli2-1*/− illustrated the altered auxin response maxima, which might be caused by the reduced translational efficiency of key auxin-related regulators of embryo development (Figure 5C), such as auxin response factor MP and transporter PIN7 (Figures 6A–6H and S9E–S9J). This similar phenomenon also occurred in the *apum24* mutant, whose abnormal embryos displayed altered auxin maxima resulting from the mislocalization of PIN1 and PIN7.[29] In addition, knocking down *RLI2* caused the decreased abundance of 40S, 60S, and 80S ribosome subunits globally (Figure 5B) and led to ribosome insufficiency, thereby affecting the ribosome assembly, which might be the reason for reduced translational efficiency. Overall, our results highlight the importance of ribosome assembly and translation regulation in gametophyte development and embryogenesis.

### Limitations of the study

Our current study revealed that RLI2 facilitates the assembly of the translational machinery to regulate *Arabidopsis* growth and development. Because of the sensitivity of proteome and the spatiotemporal expression of different proteins, we cannot detect all proteins regulated by RLI2. However, based on the phenotypes and expression profile of *RNAi-RLI2* and *rli2*+/−, we found several RLI2 downstream genes that directly regulate embryo development and other processes. Collectively, we cannot conclude whether RLI2 regulation of translational efficiency is general for all proteins or specific to some proteins. We hypothesized that RLI2 regulation may be general, but the obvious phenotypes probably arise in the rapid-growth tissues and organs (embryo, gametophyte, and apical meristem) because they need more newborn proteins. In addition, although both *Arabidopsis RLI* gene and yeast *RLI* gene regulate translational efficiency, they could not replace each other's functions. It is worth elucidating the functional divergence of RLI genes, which will provide insight into understanding the regulatory mechanism of translational efficiency between different species.

## STAR★METHODS

Detailed methods are provided in the online version of this paper and include the following:

- KEY RESOURCES TABLE
- RESOURCE AVAILABILITY
  - Lead contact
  - Materials availability
  - Data and code availability
- EXPERIMENTAL MODEL AND SUBJECT DETAILS
- METHOD DETAILS
  - Plant materials and growth conditions
  - DNA manipulation
  - RNA extraction, semi-quantitative RT-PCR, and real time-quantitative PCR
  - Pollen analysis
  - Whole-mount ovule clearing
  - Yeast complementation
  - Protein interaction assays
  - Polysome profiling and protein preparation
  - Nucleocytoplasmic separation experiment
  - Whole-mount immunolocalization assay
  - Proteome and data analysis
  - Click-iT protein reaction assay
  - RNA-seq and data analysis
- QUANTIFICATION AND STATISTICAL ANALYSIS

### SUPPLEMENTAL INFORMATION

Supplemental information can be found online at https://doi.org/10.1016/j.celrep.2023.112741.

### ACKNOWLEDGMENTS

We thank Prof. Meng-Xiang Sun (Wuhan University) for providing *pDD45*::*GFP* plant and *MCS*::*H2B-GFP* vector, and Yu-Xuan Bai (Shanghai Jiao Tong University) for discussion of the Click-iT Protein Reaction experiment. This research was supported by funding from the National Natural Science Foundation of China (32270339, 32070342), the National Basic Research Program of China (grant 2014CB943404), Shanghai Jiao Tong University JiRLMDS Joint Research Fund (project MDS-JF-2020-8), the Agri-X Interdisciplinary Fund of Shanghai Jiao Tong University (Agri-X20200204 and Agri-X2017006), the Bio-X Interdisciplinary Fund of Shanghai Jiao Tong University (20CX-04), and the Scientific and Technological Innovation Funds of Shanghai Jiao Tong University (19X160020009).

### AUTHOR CONTRIBUTIONS

W.-H.L. designed the study, supervised the project, analyzed data, wrote and edited the manuscript, and acquired funding. S.-X.Y. and L.-Q.H. designed and performed the experiments, analyzed data, and wrote and edited the manuscript. R.-B.D. helped to perform experiments. L.-H.Y. and Y.-J.Z. helped to conduct data analysis. T.Z. and Z.-P.X. helped to design and perform yeast experiments and wrote the corresponding contents in the manuscript.

### DECLARATION OF INTERESTS

The authors declare no competing interests.

### INCLUSION AND DIVERSITY

We support inclusive, diverse, and equitable conduct of research.

Received: October 19, 2022
Revised: April 1, 2023
Accepted: June 20, 2023
Published: July 6, 2023

### REFERENCES

1. Sonenberg, N., and Hinnebusch, A.G. (2009). Regulation of translation initiation in eukaryotes: mechanisms and biological targets. Cell *136*, 731–745.

2. Jackson, R.J., Hellen, C.U.T., and Pestova, T.V. (2010). The mechanism of eukaryotic translation initiation and principles of its regulation. Nat. Rev. Mol. Cell Biol. *11*, 113–127.
3. Kwan, T., and Thompson, S.R. (2019). Noncanonical Translation Initiation in Eukaryotes. Cold Spring Harbor Perspect. Biol. *11*, a032672.
4. Cairo, A., Vargova, A., Shukla, N., Capitao, C., Mikulkova, P., Valuchova, S., Pecinkova, J., Bulankova, P., and Riha, K. (2022). Meiotic exit in *Arabidopsis* is driven by P-body-mediated inhibition of translation. Science *377*, 629–634.
5. Glover, J., Grelon, M., Craig, S., Chaudhury, A., and Dennis, E. (1998). Cloning and characterization of *MS5* from *Arabidopsis*: a gene critical in male meiosis. Plant J. *15*, 345–356.
6. Pisarev, A.V., Hellen, C.U.T., and Pestova, T.V. (2007). Recycling of eukaryotic posttermination ribosomal complexes. Cell *131*, 286–299.
7. Andersen, D.S., and Leevers, S.J. (2007). The essential *Drosophila* ATP-binding cassette domain protein, pixie, binds the 40 S ribosome in an ATP-dependent manner and is required for translation initiation. J. Biol. Chem. *282*, 14752–14760.
8. Chen, Z.Q., Dong, J., Ishimura, A., Daar, I., Hinnebusch, A.G., and Dean, M. (2006). The essential vertebrate ABCE1 protein interacts with eukaryotic initiation factors. J. Biol. Chem. *281*, 7452–7457.
9. Dong, J., Lai, R., Nielsen, K., Fekete, C.A., Qiu, H., and Hinnebusch, A.G. (2004). The essential ATP-binding cassette protein RLI1 functions in translation by promoting preinitiation complex assembly. J. Biol. Chem. *279*, 42157–42168.
10. Mancera-Martínez, E., Brito Querido, J., Valasek, L.S., Simonetti, A., and Hashem, Y. (2017). ABCE1: A special factor that orchestrates translation at the crossroad between recycling and initiation. RNA Biol. *14*, 1279–1285.
11. Heuer, A., Gerovac, M., Schmidt, C., Trowitzsch, S., Preis, A., Kötter, P., Berninghausen, O., Becker, T., Beckmann, R., and Tampé, R. (2017). Structure of the 40S-ABCE1 post-splitting complex in ribosome recycling and translation initiation. Nat. Struct. Mol. Biol. *24*, 453–460.
12. Kratzat, H., Mackens-Kiani, T., Ameismeier, M., Potocnjak, M., Cheng, J., Dacheux, E., Namane, A., Berninghausen, O., Herzog, F., Fromont-Racine, M., et al. (2021). A structural inventory of native ribosomal ABCE1-43S pre-initiation complexes. EMBO J. *40*, e105179.
13. Khoshnevis, S., Gross, T., Rotte, C., Baierlein, C., Ficner, R., and Krebber, H. (2010). The iron-sulphur protein RNase L inhibitor functions in translation termination. EMBO Rep. *11*, 214–219.
14. Navarro-Quiles, C., Mateo-Bonmatí, E., and Micol, J.L. (2018). ABCE Proteins: From Molecules to Development. Front. Plant Sci. *9*, 1125.
15. Pighin, J.A., Zheng, H., Balakshin, L.J., Goodman, I.P., Western, T.L., Jetter, R., Kunst, L., and Samuels, A.L. (2004). Plant Cuticular Lipid Export Requires an ABC Transporter. Science *306*, 702–704.
16. Do, T.H.T., Martinoia, E., and Lee, Y. (2018). Functions of ABC transporters in plant growth and development. Curr. Opin. Plant Biol. *41*, 32–38.
17. Fedi, F., O'Neill, C.M., Menard, G., Trick, M., Dechirico, S., Corbineau, F., Bailly, C., Eastmond, P.J., and Penfield, S. (2017). Awake1, an ABC-Type Transporter, Reveals an Essential Role for Suberin in the Control of Seed Dormancy. Plant Physiol. *174*, 276–283.
18. Sarmiento, C., Nigul, L., Kazantseva, J., Buschmann, M., and Truve, E. (2006). AtRLI2 is an endogenous suppressor of RNA silencing. Plant Mol. Biol. *61*, 153–163.
19. Bisbal, C., Martinand, C., Silhol, M., Lebleu, B., and Salehzada, T. (1995). Cloning and characterization of a RNAse L inhibitor. A new component of the interferon-regulated 2-5A pathway. J. Biol. Chem. *270*, 13308–13317.
20. Coelho, C.M.A., Kolevski, B., Bunn, C., Walker, C., Dahanukar, A., and Leevers, S.J. (2005). Growth and cell survival are unevenly impaired in *pixie* mutant wing discs. Development *132*, 5411–5424.
21. Zhao, Z., Fang, L.L., Johnsen, R., and Baillie, D.L. (2004). ATP-binding cassette protein E is involved in gene transcription and translation in *Caenorhabditis elegans*. Biochem. Biophys. Res. Commun. *323*, 104–111.
22. Petersen, B.O., Jørgensen, B., and Albrechtsen, M. (2004). Isolation and RNA silencing of homologues of the RNase L inhibitor in *Nicotiana* species. Plant Sci. *167*, 1283–1289.
23. Kougioumoutzi, E., Cartolano, M., Canales, C., Dupré, M., Bramsiepe, J., Vlad, D., Rast, M., Dello Ioio, R., Tattersall, A., Schnittger, A., et al. (2013). *SIMPLE LEAF3* encodes a ribosome-associated protein required for leaflet development in *Cardamine hirsuta*. Plant J. *73*, 533–545.
24. Mõttus, J., Maiste, S., Eek, P., Truve, E., and Sarmiento, C. (2021). Mutational analysis of *Arabidopsis thaliana* ABCE2 identifies important motifs for its RNA silencing suppressor function. Plant Biol. *23*, 21–31.
25. Drews, G.N., and Koltunow, A.M.G. (2011). The female gametophyte. Arabidopsis Book *9*, e0155.
26. Bowman, J.L., Drews, G.N., and Meyerowitz, E.M. (1991). Expression of the Arabidopsis Floral Homeotic Gene *AGAMOUS* Is Restricted to-Specific Cell Types Late in Flower Development. Plant Cell *3*, 749–758.
27. Gifford, E.M., and Foster, A.S. (1989). Morphology and Evolution of Vascular Plants (W.H. Freeman and Company).
28. Missbach, S., Weis, B.L., Martin, R., Simm, S., Bohnsack, M.T., and Schleiff, E. (2013). 40S ribosome biogenesis co-factors are essential for gametophyte and embryo development. PLoS One *8*, e54084.
29. Shanmugam, T., Abbasi, N., Kim, H.S., Kim, H.B., Park, N.I., Park, G.T., Oh, S.A., Park, S.K., Muench, D.G., Choi, Y., et al. (2017). An Arabidopsis divergent pumilio protein, APUM24, is essential for embryogenesis and required for faithful pre-rRNA processing. Plant J. *92*, 1092–1105.
30. Shi, D.Q., Liu, J., Xiang, Y.H., Ye, D., Sundaresan, V., and Yang, W.C. (2005). *SLOW WALKER1*, essential for gametogenesis in Arabidopsis, encodes a WD40 protein involved in 18S ribosomal RNA biogenesis. Plant Cell *17*, 2340–2354.
31. Li, N., Yuan, L., Liu, N., Shi, D., Li, X., Tang, Z., Liu, J., Sundaresan, V., and Yang, W.C. (2009). *SLOW WALKER2*, a NOC1/MAK21 homologue, is essential for coordinated cell cycle progression during female gametophyte development in Arabidopsis. Plant Physiol. *151*, 1486–1497.
32. Huang, C.K., Huang, L.F., Huang, J.J., Wu, S.J., Yeh, C.H., and Lu, C.A. (2010). A DEAD-box protein, AtRH36, is essential for female gametophyte development and is involved in rRNA biogenesis in Arabidopsis. Plant Cell Physiol. *51*, 694–706.
33. Liu, M., Shi, D.Q., Yuan, L., Liu, J., and Yang, W.C. (2010). *SLOW WALKER3*, encoding a putative DEAD-box RNA helicase, is essential for female gametogenesis in *Arabidopsis*. J. Integr. Plant Biol. *52*, 817–828.
34. Cheng, P., Li, H., Yuan, L., Li, H., Xi, L., Zhang, J., Liu, J., Wang, Y., Zhao, H., Zhao, H., and Han, S. (2018). The ERA-Related GTPase AtERG2 Associated with Mitochondria 18S RNA Is Essential for Early Embryo Development in *Arabidopsis*. Front. Plant Sci. *9*, 182.
35. Chantha, S.C., Gray-Mitsumune, M., Houde, J., and Matton, D.P. (2010). The *MIDASIN* and *NOTCHLESS* genes are essential for female gametophyte development in *Arabidopsis thaliana*. Physiol. Mol. Biol. Plants *16*, 3–18.
36. Xiong, F., Duan, C.Y., Liu, H.H., Wu, J.H., Zhang, Z.H., Li, S., and Zhang, Y. (2020). Arabidopsis KETCH1 Is Critical for the Nuclear Accumulation of Ribosomal Proteins and Gametogenesis. Plant Cell *32*, 1270–1284.
37. Schneitz, K., Hulskamp, M., and Pruitt, R.E. (1995). Wild-type ovule development in *Arabidopsis thaliana*: a light microscope study of cleared whole-mount tissue. Plant J. *7*, 731–749.
38. Baud, S., Boutin, J.-P., Miquel, M., Lepiniec, L., and Rochat, C. (2002). An integrated overview of seed development in *Arabidopsis thaliana* ecotype WS. Plant Physiol. Biochem. *40*, 151–160.
39. Meinke, D., Muralla, R., Sweeney, C., and Dickerman, A. (2008). Identifying essential genes in Arabidopsis thaliana. Trends Plant Sci. *13*, 483–491.
40. Christensen, C.A., King, E.J., Jordan, J.R., and Drews, G.N. (1997). Megagametogenesis in *Arabidopsis* wild type and the *Gf* mutant. Sex. Plant Reprod. *10*, 49–64.

41. Pagnussat, G.C., Alandete-Saez, M., Bowman, J.L., and Sundaresan, V. (2009). Auxin-dependent patterning and gamete specification in the *Arabidopsis* female gametophyte. Science *324*, 1684–1689.

42. Steffen, J.G., Kang, I.H., Macfarlane, J., and Drews, G.N. (2007). Identification of genes expressed in the Arabidopsis female gametophyte. Plant J. *51*, 281–292.

43. Twell, D., Yamaguchi, J., and McCormick, S. (1990). Pollen-specific gene expression in transgenic plants: coordinate regulation of two different tomato gene promoters during microsporogenesis. Development *109*, 705–713.

44. Harrison-Lowe, N.J., and Olsen, L.J. (2008). Autophagy protein 6 (ATG6) is required for pollen germination in *Arabidopsis thaliana*. Autophagy *4*, 339–348.

45. Francis, K.E., Lam, S.Y., and Copenhaver, G.P. (2006). Separation of Arabidopsis pollen tetrads is regulated by *QUARTET1*, a pectin methylesterase gene. Plant Physiol. *142*, 1004–1013.

46. Hu, L.Q., Yu, S.X., Xu, W.Y., Zu, S.H., Jiang, Y.T., Shi, H.T., Zhang, Y.J., Xue, H.W., Wang, Y.X., and Lin, W.H. (2023). Spatiotemporal formation of the large vacuole regulated by the BIN2-VLG module is required for female gametophyte development in Arabidopsis. Plant Cell *35*, 1241–1258.

47. Li, M.W., AuYeung, W.K., and Lam, H.M. (2013). The GCN2 homologue in *Arabidopsis thaliana* interacts with uncharged tRNA and uses Arabidopsis eIF2alpha molecules as direct substrates. Plant Biol. *15*, 13–18.

48. Burks, E.A., Bezerra, P.P., Le, H., Gallie, D.R., and Browning, K.S. (2001). Plant initiation factor 3 subunit composition resembles mammalian initiation factor 3 and has a novel subunit. J. Biol. Chem. *276*, 2122–2131.

49. Jung, S.H., Kim, R.J., Kim, K.J., Lee, D.H., and Suh, M.C. (2019). Plastidial and Mitochondrial Malonyl CoA-ACP Malonyltransferase is Essential for Cell Division and Its Overexpression Increases Storage Oil Content. Plant Cell Physiol. *60*, 1239–1249.

50. He, Y., Chen, L., Zhou, Y., Mawhinney, T.P., Chen, B., Kang, B.H., Hauser, B.A., and Chen, S. (2011). Functional characterization of *Arabidopsis thaliana* isopropylmalate dehydrogenases reveals their important roles in gametophyte development. New Phytol. *189*, 160–175.

51. Locascio, A., Roig-Villanova, I., Bernardi, J., and Varotto, S. (2014). Current perspectives on the hormonal control of seed development in Arabidopsis and maize: a focus on auxin. Front. Plant Sci. *5*, 412.

52. Guo, Y., Ren, G., Zhang, K., Li, Z., Miao, Y., and Guo, H. (2021). Leaf senescence: progression, regulation, and application. Mol. Horticulture *1*, 5.

53. Benková, E., Michniewicz, M., Sauer, M., Teichmann, T., Seifertová, D., Jürgens, G., and Friml, J. (2003). Local, Efflux-Dependent Auxin Gradients as a Common Module for Plant Organ Formation. Cell *115*, 591–602.

54. Berleth, T., and Jürgens, G. (1993). The role of the *MONOPTEROS* gene in organising the basal body region of the *Arabidopsis* embryo. Development *118*, 575–587.

55. Zhang, L., Liu, X., Gaikwad, K., Kou, X., Wang, F., Tian, X., Xin, M., Ni, Z., Sun, Q., Peng, H., and Vierling, E. (2017). Mutations in eIF5B Confer Thermosensitive and Pleiotropic Phenotypes via Translation Defects in *Arabidopsis thaliana*. Plant Cell *29*, 1952–1969.

56. Xia, C., Wang, Y.J., Li, W.Q., Chen, Y.R., Deng, Y., Zhang, X.Q., Chen, L.Q., and Ye, D. (2010). The Arabidopsis eukaryotic translation initiation factor 3, subunit F (*AteIF3f*), is required for pollen germination and embryogenesis. Plant J. *63*, 189–202.

57. Zhang, Z., Guo, X., Ge, C., Ma, Z., Jiang, M., Li, T., Koiwa, H., Yang, S.W., and Zhang, X. (2017). KETCH1 imports HYL1 to nucleus for miRNA biogenesis in *Arabidopsis*. Proc. Natl. Acad. Sci. USA *114*, 4011–4016.

58. Yarunin, A., Panse, V.G., Petfalski, E., Dez, C., Tollervey, D., and Hurt, E.C. (2005). Functional link between ribosome formation and biogenesis of iron-sulfur proteins. EMBO J. *24*, 580–588.

59. Kispal, G., Sipos, K., Lange, H., Fekete, Z., Bedekovics, T., Janáky, T., Bassler, J., Aguilar Netz, D.J., Balk, J., Rotte, C., and Lill, R. (2005). Biogenesis of cytosolic ribosomes requires the essential iron-sulphur protein Rli1p and mitochondria. EMBO J. *24*, 589–598.

60. Shoemaker, C.J., and Green, R. (2011). Kinetic analysis reveals the ordered coupling of translation termination and ribosome recycling in yeast. Proc. Natl. Acad. Sci. USA *108*, E1392–E1398.

61. Kärblane, K., Gerassimenko, J., Nigul, L., Piirsoo, A., Smialowska, A., Vinkel, K., Kylsten, P., Ekwall, K., Swoboda, P., Truve, E., and Sarmiento, C. (2015). ABCE1 is a highly conserved RNA silencing suppressor. PLoS One *10*, e0116702.

62. Toompuu, M., Kärblane, K., Pata, P., Truve, E., and Sarmiento, C. (2016). ABCE1 is essential for S phase progression in human cells. Cell Cycle *15*, 1234–1247.

63. Kim, T.H., Kim, B.H., Yahalom, A., Chamovitz, D.A., and von Arnim, A.G. (2004). Translational regulation via 5' mRNA leader sequences revealed by mutational analysis of the Arabidopsis translation initiation factor subunit eIF3h. Plant Cell *16*, 3341–3356.

64. Kulichová, K., Pieters, J., Kumar, V., Honys, D., and Hafidh, S. (2022). A Plastid-Bound Ankyrin Repeat Protein Controls Gametophyte and Early Embryo Development in *Arabidopsis thaliana*. Front. Plant Sci. *13*, 767339.

65. Jin, H., Song, Z., and Nikolau, B.J. (2012). Reverse genetic characterization of two paralogous acetoacetyl CoA thiolase genes in Arabidopsis reveals their importance in plant growth and development. Plant J. *70*, 1015–1032.

66. Xu, X.M., and Møller, S.G. (2004). AtNAP7 is a plastidic SufC-like ATP-binding cassette/ATPase essential for *Arabidopsis* embryogenesis. Proc. Natl. Acad. Sci. USA *101*, 9143–9148.

67. Wu, G., Carville, J.S., and Spalding, E.P. (2016). ABCB19-mediated polar auxin transport modulates Arabidopsis hypocotyl elongation and the endoreplication variant of the cell cycle. Plant J. *85*, 209–218.

68. Li, H.M., Chen, H., Yang, Z.N., and Gong, J.M. (2012). *Cdi* gene is required for pollen germination and tube growth in Arabidopsis. FEBS Lett. *586*, 1027–1031.

69. Wu, Y., Yan, J., Zhang, R., Qu, X., Ren, S., Chen, N., and Huang, S. (2010). *Arabidopsis* FIMBRIN5, an actin bundling factor, is required for pollen germination and pollen tube growth. Plant Cell *22*, 3745–3763.

70. Wei, Q., Yang, Y., Li, H., Liu, Z., Fu, R., Feng, H., and Li, C. (2021). The xyloglucan galactosylation modulates the cell wall stability of pollen tube. Planta *254*, 133.

71. Stoppel, R., Manavski, N., Schein, A., Schuster, G., Teubner, M., Schmitz-Linneweber, C., and Meurer, J. (2012). RHON1 is a novel ribonucleic acid-binding protein that supports RNase E function in the *Arabidopsis* chloroplast. Nucleic Acids Res. *40*, 8593–8606.

72. Falcone Ferreyra, M.L., Casadevall, R., Luciani, M.D., Pezza, A., and Casati, P. (2013). New evidence for differential roles of l10 ribosomal proteins from Arabidopsis. Plant Physiol. *163*, 378–391.

73. Kim, D., Paggi, J.M., Park, C., Bennett, C., and Salzberg, S.L. (2019). Graph-based genome alignment and genotyping with HISAT2 and HISAT-genotype. Nat. Biotechnol. *37*, 907–915.

74. Pertea, M., Pertea, G.M., Antonescu, C.M., Chang, T.C., Mendell, J.T., and Salzberg, S.L. (2015). StringTie enables improved reconstruction of a transcriptome from RNA-seq reads. Nat. Biotechnol. *33*, 290–295.

75. Huang, D.W., Sherman, B.T., Tan, Q., Kir, J., Liu, D., Bryant, D., Guo, Y., Stephens, R., Baseler, M.W., Lane, H.C., and Lempicki, R.A. (2007). DAVID Bioinformatics Resources: expanded annotation database and novel algorithms to better extract biology from large gene lists. Nucleic Acids Res. *35*, W169–W175.

76. Sherman, B.T., Hao, M., Qiu, J., Jiao, X., Baseler, M.W., Lane, H.C., Imamichi, T., and Chang, W. (2022). DAVID: a web server for functional enrichment analysis and functional annotation of gene lists (2021 update). Nucleic Acids Res. *50*, W216–W221.

77. Ulmasov, T., Murfett, J., Hagen, G., and Guilfoyle, T.J. (1997). Aux/IAA proteins repress expression of reporter genes containing natural and highly active synthetic auxin response elements. Plant Cell *9*, 1963–1971.

78. Wu, J.J., Peng, X.B., Li, W.W., He, R., Xin, H.P., and Sun, M.X. (2012). Mitochondrial GCD1 dysfunction reveals reciprocal cell-to-cell signaling during the maturation of *Arabidopsis* female gametes. Dev. Cell *23*, 1043–1058.

79. Schlereth, A., Möller, B., Liu, W., Kientz, M., Flipse, J., Rademacher, E.H., Schmid, M., Jürgens, G., and Weijers, D. (2010). MONOPTEROS controls embryonic root initiation by regulating a mobile transcription factor. Nature *464*, 913–916.

80. Blilou, I., Xu, J., Wildwater, M., Willemsen, V., Paponov, I., Friml, J., Heidstra, R., Aida, M., Palme, K., and Scheres, B. (2005). The PIN auxin efflux facilitator network controls growth and patterning in *Arabidopsis* roots. Nature *433*, 39–44.

81. Clough, S.J., and Bent, A.F. (1998). Floral dip: a simplified method for Agrobacterium-mediated transformation of *Arabidopsis thaliana*. Plant J. *16*, 735–743.

82. Wang, J.G., Feng, C., Liu, H.H., Feng, Q.N., Li, S., and Zhang, Y. (2017). AP1G mediates vacuolar acidification during synergid-controlled pollen tube reception. Proc. Natl. Acad. Sci. USA *114*, E4877–E4883.

83. Johnson-Brousseau, S.A., and McCormick, S. (2004). A compendium of methods useful for characterizing *Arabidopsis* pollen mutants and gametophytically-expressed genes. Plant J. *39*, 761–775.

84. Ge, Z., Bergonci, T., Zhao, Y., Zou, Y., Du, S., Liu, M.C., Luo, X., Ruan, H., García-Valencia, L.E., Zhong, S., et al. (2017). *Arabidopsis* pollen tube integrity and sperm release are regulated by RALF-mediated signaling. Science *358*, 1596–1600.

85. Yu, S.X., Zhou, L.W., Hu, L.Q., Jiang, Y.T., Zhang, Y.J., Feng, S.L., Jiao, Y., Xu, L., and Lin, W.H. (2020). Asynchrony of ovule primordia initiation in *Arabidopsis*. Development *147*, dev196618.

86. Boeke, J.D., LaCroute, F., and Fink, G.R. (1984). A positive selection for mutants lacking orotidine-5'-phosphate decarboxylase activity in yeast: 5-fluoro-orotic acid resistance. Mol. Gen. Genet. *197*, 345–346.

87. Mustroph, A., Juntawong, P., and Bailey-Serres, J. (2009). Isolation of plant polysomal mRNA by differential centrifugation and ribosome immunopurification methods. Methods Mol. Biol. *553*, 109–126.

## STAR★METHODS

### KEY RESOURCES TABLE

| REAGENT or RESOURCE | SOURCE | IDENTIFIER |
|---|---|---|
| Antibodies | | |
| Mouse monoclonal anti-GFP | Abways | Cat# AB0005 |
| Rabbit polyclonal anti-mCherry | Proteintech | Cat# 26765-1-AP; RRID:AB_2876881 |
| Rabbit polyclonal anti-IPMDH1 | Orizymes | Cat# PAB220309 |
| Rabbit polyclonal anti-EMB3147 | Orizymes | Cat# PAB09202 |
| Mouse monoclonal anti-Tubulin | Abmart | Cat# M20045; RRID:AB_2936267 |
| Mouse monoclonal anti-Actin | ABclonal | Cat# AC009; RRID:AB_2771701 |
| Rabbit monoclonal anti-Histone H3 | ShareBio | Cat# SB-CY6587 |
| Alexa Fluor 488-conjugated AffiniPure Goat Anti-Rabbit IgG (H + L) | Jackson ImmunoResearch | Cat# 111-545-003; RRID:AB_2338046 |
| Goat anti-Mouse IgG (H + L) HRP | ShareBio | Cat# SB-AB0102 |
| Goat anti-Rabbit IgG (H + L) HRP | ShareBio | Cat# SB-AB0101 |
| Bacterial and virus strains | | |
| *Escheichia coli* DH5a | Wei Di | Cat# DL1001 |
| *Agrobacerium tumefaciens* GV3101 | Wei Di | Cat# AC1001 |
| Chemicals, peptides, and recombinant proteins | | |
| TRIzol | Invitrogen | Cat# 15596–026 |
| ClonExpress II One Step Cloning Kit | Vazyme | Cat# C112-02-AA |
| SYBR Green Real-time PCR Master mix | Toyobo | Cat# QPK-201 |
| Critical commercial assays | | |
| TIANgel Purification Kit | Tian Gen | Cat# DP219-03 |
| TIANprep Mini Plasmid Kit | Tian Gen | Cat# DP103-03 |
| FastKing RT Kit (With gDNase) | Tian Gen | Cat# KR116-02 |
| NEBridge Golden Gate Assembly Kit | New England BioLabs Inc | Cat# E1601 |
| Deposited data | | |
| RNA-seq datasets | This paper | Gene Expression Omnibus in National Center for Biotechnology Information: GSE214800 |
| Proteome datasets | This paper | Integrated Proteome Resources: IPX0005285001 |
| Experimental models: Organisms/strains | | |
| Arabidopsis: *rli2-1*/+ | This paper | N/A |
| Arabidopsis: *pRLI2*::*RLI2-GFP rli2-1*/− | This paper | N/A |
| Arabidopsis: *pRLI2*::*RLI2-mCherry rli2-1*/− | This paper | N/A |
| Arabidopsis: *pES1*::*H2B-GFP* | This paper | N/A |
| Arabidopsis: *pES1*::*H2B-GFP rli2-1*/+ | This paper | N/A |
| Arabidopsis: *pUBQ10*::*RNAi-RLI2* | This paper | N/A |
| Arabidopsis: *pRLI2*::*H2B-GFP* | This paper | N/A |
| Arabidopsis: *pRLI2*::*GUS* | This paper | N/A |
| Arabidopsis: *pRLI2*::*MmRLI1-GFP* | This paper | N/A |
| Arabidopsis: *pRLI2*::*ScRLI1-GFP* | This paper | N/A |
| Yeast: *BY4741 rli1*△::*hphMX6* + *pRS416-pADH3-ScRLI1* | This paper | N/A |
| Yeast: *BY4741* (*WT*) + *pRS416-pADH3-ScRLI1* | This paper | N/A |

(*Continued on next page*)

*Continued*

| REAGENT or RESOURCE | SOURCE | IDENTIFIER |
|---|---|---|
| Yeast: *BY4741 rli1 △::hphMX6 + pRS416-pADH3-ScRLI1 + pRS415* | This paper | N/A |
| Yeast: *BY4741 rli1 △::hphMX6 + pRS416-pADH3-ScRLI1 + pRS415-pADH3-ScRLI1* | This paper | N/A |
| Yeast: *BY4741 rli1 △::hphMX6 + pRS416-pADH3-ScRLI1 + pRS415-pADH3-AtRLI2* | This paper | N/A |
| Yeast: *BY4741 rli1 △::hphMX6 + pRS416-pADH3-ScRLI1 + pRS415-pADH3-AtRLI1* | This paper | N/A |
| Oligonucleotides | | |
| See Data S4 for oligonucleotide information | This paper | N/A |
| Recombinant DNA | | |
| See Data S4 for Recombinant DNA information | This paper | N/A |
| Software and algorithms | | |
| HISAT2 | Kim et al.[73] | http://daehwankimlab.github.io/hisat2 |
| StringTie | Pertea et al.[74] | http://ccb.jhu.edu/software/stringtie |
| DAVID | Huang et al.[75]; Sherman et al.[76] | https://david.ncifcrf.gov/summary.jsp |
| GraphPad Prism7 | GraphPad | https://www.graphpad.com/features |

## RESOURCE AVAILABILITY

### Lead contact

Further information and requests for resources and reagents should be directed to and will be fulfilled by the lead contact, Wen-Hui Lin (whlin@sjtu.edu.cn).

### Materials availability

All unique/stable reagents generated in this study are available from the lead contact with a completed Materials Transfer Agreement.

### Data and code availability

- RNA-seq data are available at GEO in NCBI (https://www.ncbi.nlm.nih.gov/geo/) under accession numbers GSE214800. Proteome data are available in Integrated Proteome Resources (https://www.iprox.cn/) under accession number IPX0005285001.
- This paper does not report original code.
- Any additional information required to reanalyze the data reported in this paper is available from the lead contact upon request.

## EXPERIMENTAL MODEL AND SUBJECT DETAILS

The model used in this study is Arabidopsis. The wild-type used is the accession Columbia (Col-0). The various mutants used in this study have been described in the key resource table.

## METHOD DETAILS

### Plant materials and growth conditions

The Arabidopsis ecotype of Columbia (Col-0) was served as the wild-type control. The transfer DNA insertion lines CS332419 (*rli2-1*) was obtained from the Arabidopsis Biological Resource Center (The Ohio State University, Columbus; http://www.Arabidopsis.org). Other materials, including *DR5rev-GFP*,[77] and *pDD45*::*GFP*,[78] *pMP*::*MP-GFP*,[79] and *pPIN7*::*PIN7-GFP*[80] have been previously described. All plants were grown in the nutrient-rich soil in a greenhouse at 22°C under 16 h light/8 h dark cycle using the fluorescent white light (90 μmol $m^{-2}$ $s^{-1}$, FSL LED T8-16-65/A22B/24 bulb) as previously described.[46] Transgenic plants were generated through agroinfiltration according to the previous report.[81] Agrobacterium was collected when its OD reached to 0.8–1.0, and resuspended in 5% sucrose solution containing 0.02% silwet L-77. Then, the final concentration of agrobacterium was adjusted to 0.8–1.0. The inflorescences of five-week-old plants were immersed into the suspension liquid for 5 min, and incubated for 24 h under dark conditions. The transformants were selected in half strength Murashige and Skoog (1/2 MS) medium (Murashige and Skoog 1962) with or without 30 μg/mL hygromycin B.

## DNA manipulation

All constructs were generated using the One Step Cloning Kit (Vazyme). A 5146 bp sequence containing the 1796 bp upstream of the *RLI2* translation start codon and the genomic fragment of *RLI2* without the stop codon was amplified with the primer pair Y147/Y130. The *RLI2g* fragment was inserted into the *pHB-X-GFP* and *pHB-X-mCherry* to generate *pRLI2*::*RLI2-GFP* and *pRLI2*::*RLI2-mCherry* vector. For *pRLI2*::*GFP* construct, the sequence of *pRLI2* was amplified with the primer pair Y147/Y506. The promoter in *pHB-X-GFP* was replaced by *ProRLI2*. The sequence of *MmRLI1* CDS and *ScRLI1* CDS was amplified with the primer pair Y422/Y423 and Y424/Y425 and inserted into *pRLI2*::*GFP* to generate *pRLI2*::*MmRLI1-GFP and pRLI2*::*ScRLI1-GFP* vector. For *pES1*::*H2B-GFP* or *pRLI2*::*H2B-GFP* vector, the sequence of *pES1* (AT5G40260) was amplified with the primer pair Y270/Y271 as reported,[82] and the sequence of *ProRLI2* was amplified with the primer pair Y131/Y132. The promoter in *MCS*::*H2B-GFP* was replaced by *pES1* or *pRLI2*. For *pRLI2*::*GUS* construct, the sequence of *pRLI2* was amplified with the primer pair Y133/Y134. The promoter in *PBI101.3* was replaced by *pRLI2*.

To generate vector *pUBQ10*::*RNAi-RLI2*, 574-bp *RLI2*-sense fragments were amplified with the primer pair Y260/Y261, the *RLI2*-antisense cDNA fragment was amplified with the primer pair Y262/Y263, and inserted into the *pTCK303*.

Regarding the Co-IP assays, to produce the destination vector *pUBQ10*::*GW-GFP* and *pUBQ10*::*GW-mCherry*, the *Pro35S* in *pHB-X-GFP* and *pHB-X-mCherry* was replaced by *pUBQ10*. Then, the fragments of *RLI2* and different *eIFs* were amplified to generate *pUBQ10*::*RLI2-GFP* and *pUBQ10*::*eIF-mCherry*, respectively. Coding sequences of *RLI2*, *eIF2α*, *eIF3b*, *eIF3e*, *eIF3f*, *eIF3h*, *eIF5*, *EF1α*, *ERF1-1*, *ERF1-2*, *ERF1-1*, *RPL23AB*, and *RPS2B* were amplified with the primer pair Y129/Y130, Y474/Y475, Y476/Y477, Y478/Y479, Y480/Y481, Y482/Y483, Y484/Y485, Y613/Y614, Y615/Y616, Y617/Y618, Y619/Y620, Y465/Y466, Y460/Y462, respectively.

Regarding the BiFC assays, the destination vectors were *pXY104*::*GW-cYFP* and *pXY106-nYFP-GW*, which were used to generate the expression vectors *pXY104*::*RLI2-cYFP* and *pXY106-nYFP-eIFs*. Coding sequences of *RLI2*, *eIF2α*, *eIF3b*, *eIF3e*, *eIF3f*, *eIF3h*, *eIF5*, *EF1α*, *ERF1-1*, *ERF1-2*, *ERF1-1*, *RPL23AB*, and *RPS2B* were amplified with the primer pair Y75/Y76, Y324/Y325, Y326/Y327, Y328/Y329, Y330/Y332, Y333/Y334, Y339/Y340, Y611/Y612, Y437/Y438, Y439/Y440, Y441/Y442, Y435/Y436, and Y458/Y459, respectively.

All PCR amplifications were performed using KOD DNA polymerase. The annealing temperature and extension times were as recommended by the manufacturer. All vectors were sequenced and analyzed using Vector NTI (Invitrogen). All primers are listed in Data S4.

## RNA extraction, semi-quantitative RT-PCR, and real time-quantitative PCR

Total RNAs were extracted from Arabidopsis roots and seedlings of 7 days after germination (DAG), leaves of 21 DAG, stems of 30 DAG, inflorescence, mature ovule, mature pollen and silique of 7 days after pollination (DAP) using TRIzol reagent (Invitrogen), after which 1 μg RNA was used to synthesize the first-strand cDNA using the FastKing RT Kit with gDNase (Tiangen) according to the manufacturer's instructions.

To identify the *rli2-1* genotype, semi-quantitative RT-PCRs (SqRT-PCR) were conducted following the procedure: 95°C 5 min, 32 cycles of 95°C 30 s, 58°C 30 s, and 72°C 1 min for *RLI2* or 28 cycles of 95°C 30 s, 58°C 30 s, and 72°C 30 s for *ACTIN2*, and 72°C 5 min. 20 μL reaction system included 10 μL 2 × mix, 1 μL cDNA, 0.5 μL forward and reverse primers (10 μM). $H_2O$ was supplemented to 20 μL. *ACTIN2* (AT3G18780) was used as an internal control. Primers were used as follows: Y13 (F1)/Y14 for wild-type *RLI2*, Y13/Y15 for *rli2-1*, Y13/Y67 (R1) for the endogenous *RLI2* and Y13/mCherry for the exogenous *RLI2* in *RLI2g-mCherry;rli2-1* background, Y69/Y70 for *ACTIN2*.

To analyze the expression pattern of *RLI2*, real time-quantitative PCR (RT-qPCR) was performed with the qTOWER3G touch real-time system. 10 μL reaction system contained 5 μL SYBR Green real-time PCR master mix (Toyobo), 4.8 μL cDNA, and 0.2 μL primers. The PCR procedure was as follows: 95°C 5 min and 45 cycles of 95°C 10 s, 58°C 15 s, and 72°C 20 s. The results were processed by $2^{-\triangle\triangle Ct}$ and the differences were analyzed by t test. All experiments were completed with three independent biological replicates, each comprising three technical replicates. All primers are listed in Data S4.

## Pollen analysis

Alexander's staining of pollen was according to the previously described method.[83] The stock solution for Alexander's stain (10 mL 95% ethanol, 5 mL 1% malachite green in 95% ethanol, 5 g of phenol, 5 mL 1% acid fuschin in $H_2O$, 0.5 mL 1% orange G in $H_2O$, 2 mL glacial acetic acid, 25 mL glycerol and 50 mL $H_2O$) dilute 1:50 in $H_2O$ to working concentration. The flower at stage 12c was immersed in Alexander's work buffer overnight. The anthers and pollen grains were examined using the Axio Imager M2 (Zeiss) microscope. For DAPI staining, the pollen grains were stained with 1 μg/mL DAPI work solution for 10 min. The pollen grains were examined using the Axio Imager M2 (Zeiss) microscope. *In vitro* pollen germination was performed on germination solid medium (1 mM $CaCl_2$; 1 mM $Ca(NO_3)_2 \cdot 4H_2O$; 1 mM $MgSO_4$; 0.01% $H_3BO_3$; 0.9% Agar; pH 7.0) for 4 h at 28°C. For *in vivo* pollen tube growth assay, one pollen tetrad was collected from freshly opened flower of *pLat52*::*GUS qrt1* or *pLat52*::*GUS qrt1 rli2-1*/+ lines, and pollinated to wild-type pistils that had been emasculated 12–24 h earlier.[84] 24 h later, siliques were harvested for GUS histochemical staining. GUS staining and SEM were performed as previously described.[85]

### Whole-mount ovule clearing

Ovules were examined by CLSM according to the previously described method.[40] Dissected pistils were fixed under vacuum conditions for 30 min in 4% glutaraldehyde prepared in 12.5 mM cacodylate (pH 6.9), after which they were incubated in the fixative solution at room temperature overnight. Samples were dehydrated in the following ethanol series: 10%, 20%, 40%, 60%, 80% and 90% (10 min per step). After overnight incubation in 90% ethanol, the tissues were washed twice for at least 10 min in 100% ethanol until they were completely decolorized. The tissues were cleared in 2:1 (v/v) benzyl benzoate: benzyl alcohol for at least 1 h. Ovules were separated from pistils and mounted in immersion oil, after which they were examined using the Ni-E A1 HD25 (Nikon) microscope at excitation and emission wavelengths of 488 nm and 505–550 nm, respectively.

### Yeast complementation

This experiment was designed following the published methods.[9,86] The knockout vector (*pUC19-pScRLI1-hphMX6-tScRLI1*) was generated by transferring the 1000 bp promoter (pF/pR) and 1000 bp terminator (tF/tR) fragments of *ScRLI1* to the knockout backbone. The centromere vector (*pRS416-pADH3-ScRLI1*) was constructed by inserting the *ScRLI1* ORF region (ScF1/ScR1) to the *pRS416* backbone. The complementation vectors (*pRS415-pADH3-RLIs*) of *ScRLI1* (ScF2/ScR2), *AtRLI1* (A1F/A1R) and *AtRLI2* (A2F/A2R) were produced by cloning their ORFs to the *pRS415* backbone, respectively. Yeast strain BY4741 was used as the template to amplify the *ScRLI1* genomic DNA. These constructions were performed using NEBridge Golden Gate Assembly Kit (E1601). Primers used were provided in the Data S4.

To produce the knockout *scrli1* strain, *pRS416-pADH3-ScRLI1* vector was first introduced into the haploid strain BY4741 to select the transformant on SD + CA-Ura medium. Then the linearized knockout vector was introduced into the above transformant to select the purpose transformant on YPD medium with 300 mg/L Hygromycin B. The deleted strain for chromosomal *ScRLI1* but carrying plasmid *pRS416-pADH3-ScRLI1* was identified. To generate the complementation strains, *pRS415-RLIs* vectors were introduced into the BY4741 *rli1*△::*hphMX6* + *pRS416-pADH3-ScRLI1* strain, respectively. The final transformants were selected on SD-Leu medium and grown on SD media containing 5′-fluoro-orotic acid (5-FOA) to evict *pRS416-pADH3-ScRLI1* (negative selection for URA3).

### Protein interaction assays

For BiFC analysis, associated vectors were transformed into *Agrobacterium tumefaciens* strain GV3101 cells, which were then used to infiltrate *Nicotiana benthamiana* tobacco leaf epidermal cells. The tobacco leaves were incubated in darkness for 48–72 h and YFP fluorescence was examined by confocal microscopy (Nikon Ni-E A1 HD25).

For the co-immunoprecipitation assay, 0.1 g Arabidopsis leaves co-expressing *pUBQ10*::*RLI2-GFP* and *pUBQ10*::*eIFs-mCherry* were collected. Leaf cell pellets were resuspended in lysis buffer NB1 (50 mM Tris-HCl, pH 8.0, 500 mM sucrose, 1 mM $MgCl_2$, 10 mM EDTA, 5 mM DTT, 2 mM PMSF, and 1× protease inhibitor Cocktail) and lysed on ice for 30 min. The solution was centrifuged at 12,000 rpm for 1 h at 4°C, after which the supernatant was collected and filtered through two layers of Miracloth (Calbiochem) to completely remove cellular debris. The proteins were incubated with 10 μL pre-washed anti-GFP-conjugated beads (Chromoek) for 3 h at 4°C. After six washes with NB1 buffer, the beads were mixed with loading buffer and boiled at 100°C for 10 min. A 30 μL aliquot of each boiled sample was analyzed by Western blot using an anti-mCherry antibody (Proteintech; 1:3,000 dilution) and an anti-GFP antibody (Abways; 1:3,000 dilution). In addition, anti-Tubulin antibody (Abmart; 1:3,000 dilution) was used in Figures 5G, 6G, and S9I. The secondary antibodies used in all Western blot analysis were Goat anti-Mouse IgG (H + L) HRP (ShareBio; SB-AB0102; 1:5,000) or Goat anti-Rabbit IgG (H + L) HRP (ShareBio; SB-AB0101; 1:5,000).

### Polysome profiling and protein preparation

For polysome profiling analysis, 2 g 10 DAG seedlings of wild-type and *pUBQ10*::*RNAi-RLI2 #5* and *#12* were collected for three biological replicates and put in liquid nitrogen immediately, and then ground into powder using Multi sample freeze grinder (Wonbio-Mini). Seedling powders were resuspended in the precooled polysome extraction buffer (0.2 M Tris-HCl, pH 9.0; 0.2 M KCl; 25 mM EGTA; 35 mM $MgCl_2$; 1% Brij-35; 1% Triton X-100; 1% NP40; 1% Tween 20; 1% Sodium deoxycholate; 1% Polyoxyethylene 10 tridecyl ether; 5 mM DTT; 1 mM PMSF; 50 μg/mL CHX; 50 μg/mL Chloramphenicol; 400U/ml RNase inhibitor) according to the previous report[87] to extract total ribosomes. The samples were centrifuged at 12,000 rpm for 15 min at 4°C, the mixture was filtered through two layers of sterile Miracloth (Calbiochem). The mixture was put on ice for 10 min and centrifuged at 12,000 rpm for 15 min at 4°C. The supernatant was removed to the centrifuge tube containing prepared sucrose gradient (10%–60%, the sucrose was dissolved in sucrose salts: 40 mM Tris-HC1, pH 8.4; 20 mM KCl; 10 mM $MgCl_2$), which was prepared by gradient master (Biocomp 108) according to the manufacturer's instructions. The samples were centrifuged at 35000 rpm for 3.5 h at 4°C in a Beckman Optima XPN-100 ultracentrifuge (SW41Ti Rotor). The ribosome fractions were collected and the absorbance was analyzed by a position gradient fractionator (Biocomp 152). 2 volumes of 99% ethanol were added to the isolated polysome fractions, mixed well and allowed to stand at 4°C overnight. The mixture was centrifuged at 16,000 g for 15 min at 4°C and washed once with 70% ethanol. Pellets were resuspended in 2 × SDS loading buffer, and loaded on an SDS polyacrylamide gel.[87]

### Nucleocytoplasmic separation experiment

2 g seedlings of *pUBQ10*::*RLI2-mCherry* were collected at 10 DAG. Grind the samples with liquid nitrogen. The samples were transferred to a pre-cooled centrifuge tube, add 4 mL of Honda buffer (20 mM Tris-HCl, pH 6.8; 10 mM $MgCl_2$; 25% glycerol; 250 mM sucrose; 10 mM KCl; 1% Triton X-100; 2 mM EDTA; 1 × Protease Inhibitor Cocktail; 5 mM DTT; 20 mM β-mercaptoethanol) to mix. The samples were filtered through Miracloth filter cloth, and placed on ice for 15 min. Take 100 μL of sample as total protein. Centrifuge at 1500 g for 5 min at 4°C, the supernatant was transferred to a new tube as the cytoplasmic fraction. Wash the pellet 5 times and resuspend the pellet with Honda buffer. The collected pellet is the nuclear fraction. Resuspend the pellet in 100 μL Honda buffer. The total protein, cytoplasmic fraction, and nuclear fraction were mixed with loading buffer and boiled at 100°C for 10 min. A 30 μL aliquot of each boiled sample was analyzed by Western blot using anti-Actin antibody (ABclonal; 1:3,000 dilution), anti-mCherry antibody (Proteintech; 1:3,000 dilution), and anti-Histone H3 antibody (ShareBio; 1:3,000 dilution).

### Whole-mount immunolocalization assay

Roots were collected at 7 DAG, fixed and conducted according to the previously reported method.[46] EMB3147 (Orizymes; PAB09202) and IPMDH1 (Orizymes; PAB220309) primary antibodies were used at a dilution of 1:100. An Alexa Fluor 488-conjugated AffiniPure Goat Anti-Rabbit IgG (H + L) secondary antibody (Jackson ImmunoResearch) was used at a dilution of 1:300. Fluorescence was observed using a confocal laser scanning microscopy (Nikon Ni-E A1 HD25).

### Proteome and data analysis

The proteome samples were collected from wild type and *pUBQ10*::*RNAi-RLI2 #12*, total proteins were isolated from seedlings of 7 DAG. More than 2 g of seedlings were collected with two biological replicates. Samples using SDT (4% SDS; 100mM Tris-HCl, pH 7.6; 0.1 M DTT) lysis method to extract proteins. Protein quantification was then performed using the BCA method. Protein from each sample was digested with trypsin using the Filter aided proteome preparation (FASP) method, and the peptides were desalted using a C18 Cartridge. The peptides were lyophilized and reconstituted by adding 40 μL of 0.1% formic acid solution. Each sample was separated using the NanoElute HPLC liquid system at nanoliter flow rates. The samples were chromatographically separated and analyzed by mass spectrometry using a timsTOF Pro mass spectrometer. The raw data of mass spectrometry analysis were RAW files, and MaxQuant software (version number 1.6.14) was used for library identification and quantitative analysis. All data were provided by Personalbio.

### Click-iT protein reaction assay

14 DAG seedlings of wild-type and *pUBQ10*::*RNAi-RLI2* were cultured in 1/2 MS liquid medium containing 25 μM Click iT AHA (Invitrogen) or DMSO (mock) for 1 h. Equal amounts of seedlings were collected and put in liquid nitrogen and ground into a powder. The examples were resuspended in RIPA buffer (10 mM Tris-HCl, pH 7.5; 1 mM EDTA; 0.5% Triton X-100; 140 mM NaCl; 0.1% SDS; 0.1% sodium deoxycholate; 1 × cocktail; 1 mM PMSF; 10 μM MG132) followed by adding 10 μM DBCO-Cy5, and reacted for 30 min at room temperature. Then above examples were added 4 × SDS loading buffer without bromophenol bule to stop the reaction and centrifuged at 12000 rpm for 10 min at 4°C. The supernatant were boiled for 10 min, and the examples were separated on 4–20% SDS-PAGE. The images were taken by Typhoon RGB (Amersham). Then the same gel was stained by Coomassie brilliant blue as control.

### RNA-seq and data analysis

The RNA-seq samples were collected from wild type and *pUBQ10*::*RNAi-RLI2 #12*, total RNAs were isolated from seedlings of 7 DAG. More than 50 mg of seedlings were collected with three biological replicates. RNA integrity was assessed on an Agilent 2100 Bioanalyzer (Agilent). Sequencing libraries were prepared with the TruSeq RNA Sample Preparation Kit (Illumina) and sequenced on a HiSeq 2000 (Illumina) according to the manufacturer's standard protocols. The quality-filtered reads were mapped to the Arabidopsis Information Resource (TAIR10) version of the Arabidopsis genome by Hisat2 open-source software,[73] which is freely available at http://daehwankimlab.github.io/hisat2/. StringTie (http://ccb.jhu.edu/software/stringtie) calculates the FPKM value of each gene/transcript in the sample based on the comparison result of the Hisat2 software, and uses this value as the expression level of the gene/transcript in the sample, StringTie is freely available as open source software at http://ccb.jhu.edu/software/stringtie.[74] The DEGs were identified by the absolute value of $\log_2$ (fold change) $\geq$ 1.0 and $p \leq 0.05$ (t test). All data were provided by Origingene. Identification of significantly (hypergeometric test; FDR <0.01) enriched GO categories was done using DAVID, a web-based tool and database for KEGG and GO analysis (https://david.ncifcrf.gov/summary.jsp).

## QUANTIFICATION AND STATISTICAL ANALYSIS

Data in figures was expressed as mean ± SD. Replicates in different experiments were stated in corresponding Figure legends. Statistical analyses were performed using GraphPad Prism software (version 7.0). Statistical significance is determined by Student's t test. $p < 0.05$ were considered as statistical significantly.